

NRC Publications Archive Archives des publications du CNRC

RPAS operator guidance and safety assurance tools for the urban environment: phase II

Barber, Hali; Wall, Alanna; Tabachnick, Isaac

For the publisher's version, please access the DOI link below. / Pour consulter la version de l'éditeur, utilisez le lien DOI ci-dessous.

Publisher's version / Version de l'éditeur:

<https://doi.org/10.4224/40002761>

Laboratory Technical Report (National Research Council of Canada. Aerospace Research Centre. Aerodynamics Laboratory; no. LTR-AL-2022-0010, 2022-05-31

NRC Publications Archive Record / Notice des Archives des publications du CNRC :

<https://nrc-publications.canada.ca/eng/view/object/?id=8c40584e-afed-41b9-9a2e-5e6b851615ae>

<https://publications-cnrc.canada.ca/fra/voir/objet/?id=8c40584e-afed-41b9-9a2e-5e6b851615ae>

Access and use of this website and the material on it are subject to the Terms and Conditions set forth at

<https://nrc-publications.canada.ca/eng/copyright>

READ THESE TERMS AND CONDITIONS CAREFULLY BEFORE USING THIS WEBSITE.

L'accès à ce site Web et l'utilisation de son contenu sont assujettis aux conditions présentées dans le site

<https://publications-cnrc.canada.ca/fra/droits>

LISEZ CES CONDITIONS ATTENTIVEMENT AVANT D'UTILISER CE SITE WEB.

Questions? Contact the NRC Publications Archive team at

PublicationsArchive-ArchivesPublications@nrc-cnrc.gc.ca. If you wish to email the authors directly, please see the first page of the publication for their contact information.

Vous avez des questions? Nous pouvons vous aider. Pour communiquer directement avec un auteur, consultez la première page de la revue dans laquelle son article a été publié afin de trouver ses coordonnées. Si vous n'arrivez pas à les repérer, communiquez avec nous à PublicationsArchive-ArchivesPublications@nrc-cnrc.gc.ca.

UNPROTECTED

AIRC-CMRC

RPAS operator guidance and safety assurance tools for the urban environment – Phase II

LTR-AL-2022-0010

May 31, 2022

Hali Barber, Alanna Wall, Isaac Tabachnick

Aerospace Research Centre



National Research
Council Canada

Conseil national de
recherches Canada

Canada

AERODYNAMICS LABORATORY

RPAS operator guidance and safety assurance tools for the urban environment – Phase II

Report No.: LTR-AL-2022-0010

Date: May 31, 2022

Authors: Hali Barber, Alanna Wall, Isaac Tabachnick

Classification: Unprotected
For: Transport Canada

Distribution: Unlimited

Project #: A1-017743
Submitted by: Michael Benner, **Director of Research and Development, Aerodynamics**
Approved by: Ibrahim Yimer, **Director General, NRC Aerospace Research Centre**

Pages: 58
Figures: 27

Copy No:
Tables: 9

This report may not be published wholly or in part without the written consent of the National Research Council Canada

Executive Summary

For the second year of the RPAS operator guidance and safety assurance tools for the urban environment project, between TC and NRC, two sub-projects were carried out. The first sub-project included wind tunnel testing to evaluate the flow-fields of four urban models to determine the magnitude and locations of extreme airflow features identified as potentially hazardous to RPAS operations. The characteristics of interest measured for the four urban models representing Canadian cities were speed, direction, shear, turbulence and vorticity ($S_1 D S_2 T V$). The scope of this current phase of work included analysis of the results of two out of the five urban airflow features, specifically speed and turbulence ($S_1 T$).

Key findings from the urban airflow results included:

- For locations where airflow was not within tall building wakes, the upstream wind speed vertical gradient persisted from outside of the urban site into the urban environment at the small RPAS maximum altitude limit of 122m (400 ft);
- For locations within building wakes or wake interaction, the upstream wind speed vertical gradient was not evident within the urban environment as results showed high variability with minimal height-to-speed correlation;
- For all city models, locations were found where lateral wind speed tripled over a full scale distance of 18 m, where measurement locations crossed building wakes; and,
- High wind speeds and extreme turbulence intensities between 26% and 33% were found in the wakes of tall high-rise buildings.

The urban airflow test turbulence intensity results were used to determine full scale flow conditions for the second sub-project, a wind tunnel test where five off-the-shelf small RPAS were evaluated for flight stability for a range of turbulence. The wind speed limit for stable flying for each RPAS was found for a range in wind -speed and -turbulence intensity determined by the ability of the auto-pilot to maintain hover position. Results indicated that:

- The wind speed limit was sensitive to a range of turbulence intensity that is typical for urban airflow;
- All of the models tested were affected by turbulence intensity to a similar degree; and,
- The internal log file results recorded by the RPAS sensors during each test suggest an increase in airflow turbulence intensity causes an increase in variation of RPAS control moment, decreasing attitude controllability, thereby reducing the wind speed limit at which the RPAS could maintain position.

When the results are graphed for wind speed versus turbulence the trendline of the RPAS wind speed limit can be compared to the urban airflow results. The relationship was used to develop a method for determining an estimated wind speed limit at which the tested RPAS could avoid urban airflow instability for the four representative Canadian cities. The estimated safe wind speed limits suggest that conditions within Canadian urban environments will exist that the tested RPAS manufacturer-specified sustained wind speed tolerance does not take into account. Specifically, the intensity of turbulence for high winds in the wake of tall buildings is expected to cause a loss of attitude controllability, lowering the wind tolerance to below that of the specified value.

Contents

Executive Summary	v
List of Figures	viii
List of Tables	ix
List of Symbols	x
List of Acronyms	xi
 1. Introduction	 1
1.1 Objectives	2
1.2 Project Structure	2
 2. Urban Airflow Characterization	 3
2.1 NRC 3 m × 6 m Wind Tunnel	3
2.2 Flow Conditioning for Urban Boundary Layers	3
2.3 Urban Models	7
2.4 Instrumentation	9
2.5 Data Processing	10
2.5.1 Test Conditions	10
2.5.2 Cobra Probe Data	10
2.6 Airflow Characterization Program	14
 3. Urban Airflow Measurement Results	 17
3.1 Speed Results	17
3.1.1 Speed Gradient	17
3.1.2 Variation in Wind Speed	18
3.1.3 Local Wind-speed-ratio	21
3.2 Turbulence Intensity Results	22

4. Testing of Small RPAS	29
4.1 Flow Conditioning for Turbulence Intensity	29
4.2 RPAS Models and Flight Settings	33
4.3 RPAS Flight Procedures	33
4.4 Data Collection System and Post Processing	35
5. Small RPAS Test Matrix and Results	37
6. Evaluation of the Relationship Between the sRPAS Wind Speed Limit Results and the Urban Airflow Results	42
7. Summary and Next Steps	50
7.1 Urban Airflow Characterization	50
7.2 sRPAS Wind Tunnel Test	51
7.3 Evaluation of sRPAS Wind Tunnel Results when Compared to the Urban Airflow Results	51
References	53
A. Appendix A	55

List of Figures

2.1 Flow conditioning development study test setup.	4
2.2 OPS and SUB normalized mean flow profiles.	5
2.3 Schematic of the wind tunnel setup for urban flow-field measurements.	6
2.4 Example test configuration for each city model.	8
2.5 Urban airflows measurement system.	9
2.6 Example of probability distribution and Gaussian fit for a data point with 1.2% OOR.	11
2.7 Example of probability distribution and Gaussian fit for a data point with 40% OOR.	12
2.8 Example of probability distribution and Gaussian fit for a data point with 66% OOR.	13

3.1	Experimental results of normalized mean wind speed, U_{mean} .	19
3.2	Cases of extreme urban flow mean wind speed variation.	20
3.3	Experimental results of local wind-speed-ratio within the urban environment.	22
3.4	Experimental results of turbulence intensity, I_u .	23
3.5	Location of extreme I_u for Toronto, case: TOR:270:HPA.	25
3.6	Location of extreme I_u for Vancouver, case: VAN:160:CTR.	26
3.7	Location of extreme I_u for Halifax, case: HAL:155:SHE.	26
3.8	Location of extreme I_u for the Artificial city, case: ART:90:MD2.	27
4.1	Cases of extreme urban flow mean wind speed variation.	30
4.2	TU4 turbulence intensity contour plot results measured for a wind speed of 15 m/s.	31
4.3	Turbulence generator results for five downstream locations.	32
4.4	Wind tunnel test: RPAS models in headwind orientation.	33
4.5	Wind tunnel video recording examples.	35
5.1	RPAS test results: wind speed limit versus turbulence intensity.	39
5.2	Pitch motor ratio and roll motor ratio for the Matrice 300 in SMT-0-incr and TU4-0-incr flow configurations.	40
6.1	Urban wind-speed and -turbulence instability avoidance graph for the Mavic 2 Zoom.	43
6.2	Schematic of urban and open terrain wind speed profile relationship.	45
6.3	Urban wind-speed and -turbulence instability avoidance graph for the Mavic 2 Zoom: Toronto, all data points.	48
6.4	Sample urban wind-speed and -turbulence instability avoidance graph.	49

List of Tables

2.1	Test matrix: Toronto.	16
3.1	Maximum results for I_u .	24
3.2	Average I_u results for each urban height reference colour in Figure 3.4.	28

4.1	RPAS wind tunnel flight settings.	34
5.1	RPAS wind tunnel test matrix and results.	38
6.1	Urban wind-speed and -turbulence instability avoidance results.	46
A.1	Test matrix: Vancouver.	56
A.2	Test matrix: Halifax.	57
A.3	Test matrix: Artificial city.	58

Symbols

A	frontal area of wake generator [m^2]
BL	back left motor speed
BR	back right motor speed
D	characteristic length, building width [m]
h	small spire height [mm]
H	large spire height [mm]
I_u	normalized turbulence intensity [-]
FL	front left motor speed
FR	front right motor speed
Re	Reynolds number
SMT_{Limit}	smooth flow condition speed limit [m/s or km/h]
U	wind speed [m/s]
U_{mean}	normalized mean wind speed [-]
$U_{N1.0}$	relative sRPAS wind speed limit at $U_{mean} = 1.0$ [-]
U_{10}	hourly mean wind speed reported by a weather station [m/s]
U_{122}	mean wind speed at 122 m above ground [m/s]
U_z	wind speed at an above ground height, z , [m/s]
x	streamwise distance between turbulence generator and measurement plane [m]
y	lateral distance [m]
z	height above ground [m]
α	power law exponent [-]
β	flow angle [$^\circ$]
ϵ	kinematic viscosity [m^2/s]

γ	normalized U_{mean} at $I_u = 0$ [-]
ϕ	Gaussian function of the flow angle β
$\bar{\beta}$	fitted mean flow angle [°]
σ_β	fitted standard deviation of the flow angle [°]
$\hat{\phi}$	magnitude of the Gaussian probability peak

Acronyms

ABL	atmospheric boundary layer
AVE	measurement plane: avenue location
CAAM	Canadian Advanced Air Mobility Consortium
CARs	Canadian Aviation Regulations
CHA	measurement plane: building channel location
CTR	measurement plane: central location
FS	full scale
HPA	measurement plane: horizontal flight path location
IAM	Integrated Autonomous Mobility
JET	measurement plane: accelerated flow location
MD1	measurement plane: modular building arrangement 1
MD2	measurement plane: modular building arrangement 2
MD3	measurement plane: modular building arrangement 3
MD4	measurement plane: modular building arrangement 4
NRC	National Research Council Canada
OOD	out-of-range
OPS	ABL over open-suburban terrain
RPAS	remotely piloted aircraft systems
RPM	revolution per minute
RWDI	Rowan Williams Davies & Irwin Inc.
$S_1 D S_2 T V$	speed direction shear turbulence vorticity
SHE	measurement plane: vortex shedding location
SMEs	small and mid-size enterprises
sRPAS	small remotely piloted aircraft systems
std	standard deviation
SUB	ABL over suburban terrain
SWT	sustained wind speed tolerance
TC	Transport Canada
U-I	U_{mean} versus I_u
VOR	measurement plane: rooftop vortex location
VPA	measurement plane: vertical flight path location

1. Introduction

With the rapid growth of the remotely piloted aircraft systems (RPAS) industry world-wide, factors affecting flight stability and endurance are becoming increasingly important for safe RPAS operation, particularly for flying within urban environments where risk of harm to people on the ground is of primary concern. In Canada, the fast pace at which the RPAS industry is developing the technology and infrastructure to use RPAS in the urban environment has been made public by RPAS groups promoting urban air mobility (CAAM and NEXA Advisors, 2021). Trials of use cases are making headlines, including transfer of small cargo between inner-city hospitals (Deschamps, 2021) and small package delivery services (Kulisch, 2021). The type of use cases are indicating that small remotely piloted aircraft systems (sRPAS) will become the first weight category ($0.25 \text{ kg} < \text{RPAS} < 25 \text{ kg}$) for autonomous air transportation in cities, with larger RPAS to follow.

Although it is prudent for operators to avoid flying in adverse weather, as the industry develops to include routine flights and first responder RPAS capabilities within cities, safe operating limits will need to be identified to ensure successful urban flight planning to avoid collision with people or structures.

The purpose of this multi-phase project is to support Transport Canada (TC) with the development of knowledge and tools to promote RPAS operator awareness and safety assurance for flight within the urban environment. This project is a collaboration between TC and National Research Council Canada (NRC), with limited contribution from Canadian small and mid-size enterprises (SMEs) developing expertise in urban infrastructure for RPAS (Rowan Williams Davies & Irwin Inc. (RWDI)) and urban RPAS operations (IndroRobotics). The intention of the project is to develop scientific knowledge of Canadian urban airflow and to evaluate the effects of adverse urban airflow characteristics on RPAS.

The first year, Phase I, of this collaboration included categorization of flow types within the urban environment that are expected to challenge RPAS operation. Description and illustration of the flow types have been provided to TC by the NRC in video format titled *Urban Airflow: What Drone Pilots Need to Know*, (Transport Canada, 2021) and a companion report (Barber and Wall, 2020). The five urban airflow types identified during Phase I as potentially hazardous to RPAS are: speed, direction, shear, turbulence and vorticity ($S_1 D S_2 T V$).

To build upon the understanding of the hazardous urban airflow types and their impact on safe RPAS operation, for the second year, Phase II, wind tunnel testing was used to evaluate urban airflow to determine the extreme magnitudes of each flow type for Canadian cities, and test RPAS flight within the extremes of two flow types; speed and turbulence. The RPAS flight test included small RPAS, or sRPAS, with a range in weight and drone system sophistication. Description and results of the urban airflow tests and the RPAS wind tunnel tests are presented in this report.

1.1 Objectives

The TC RPAS Task Force and the NRC Integrated Autonomous Mobility program (Integrated Autonomous Mobility (IAM)) both have objectives for Phase II to evaluate the effects of Canadian urban airflow on RPAS operations to support:

- TC Objective: Regulatory development of the Canadian Aviation Regulations (Canadian Aviation Regulations (CARs)) and Standards Part IX - Remotely Piloted Aircraft Systems for urban operations using:
 - Measured flow characteristics in representative Canadian cities; and
 - Measured RPAS response to typical urban flow characteristics.
- TC and NRC Objective: Identify adverse wind effects on RPAS operations within the urban environment for Canadian applications to support the growing RPAS industry including operators and manufacturers.
- NRC Objective: To support existing industrial and academic partnerships with Carleton University, Royal Military College and Canadian SME, RWDI toward the development of Highly Qualified Personnel and technologies to support RPAS operation in cities.

Beyond the direct input towards understanding of urban airflow impacts on RPAS for regulatory consideration, the shared knowledge from this Phase of work is expected to provide working groups within the NRC and other invested groups such as the Canadian Aviation Air Mobility (Canadian Advanced Air Mobility Consortium (CAAM)) with data on urban airflow characteristics that can be directly adapted for related projects.

1.2 Project Structure

The project structure for this Phase included evaluating the extremes of urban airflow characteristics identified in Phase I, for Canadian cities, and the reaction of sRPAS to two of those airflow characteristics. Phase II included two wind tunnel test campaigns:

- Part 1: measurement of a large sample of urban airflow characteristics for Canadian cities; and
- Part 2: evaluation of the stability of sRPAS within urban airflows for wind-speed and -turbulence.

Details of the Part 1 test setup and results are presented in Chapter 2 and 3, the test setup and results of Part 2 are presented in Chapter 4 and 5. Chapter 6 will present the evaluation of the relationship between the sRPAS wind speed limit and urban airflow. Finally, Chapter 7 presents the summary and next steps for the project.

2. Urban Airflow Characterization

In the following sections, the test setup, procedures and results used to evaluate Canadian urban airflow are presented. Some results and test setup details are reported in relation to the altitude limits for the small RPAS (sRPAS) category according to the current Canadian Aviation Regulations Part IX, which is 122 m (400 ft) above ground. This has been done to:

- highlight the comparison of the Phase II, Part 1 results to the guidance provided in the Phase I report and video, Urban Airflow: What Drone Pilots Need to Know; and
- to relate directly to the flow conditions for the sRPAS wind tunnel test matrix for Part 2 of Phase II, reported in Chapter 5.

For the urban airflow characterization wind tunnel testing, a complex test setup was required to measure representative urban airflow accurately within the flow-field of each of the four city models. The following section explains the wind tunnel setup, flow conditioning for urban boundary layers, urban models, instrumentation, data processing and test program.

2.1 NRC 3 m × 6 m Wind Tunnel

The experimental work was carried out at the NRC 3 m × 6 m Wind Tunnel in Ottawa, Canada. The wind tunnel is an open-circuit facility with a 3.1 m wide × 5.4 m high × 6.4 m long test section and a 2.9 m diameter model turntable. The size of the test section and large turntable make the tunnel ideal for testing urban models at typical scales of between 1:200 and 1:500 (Irwin *et al.*, 2005) for a full range of possible wind angles.

2.2 Flow Conditioning for Urban Boundary Layers

Prior to testing flows within the city models, a test section flow conditioning study was carried out to ensure real-world representation.

For scaled testing of flow-field models representing atmospheric conditions, upstream flow disturbance objects are placed in front of the model, within a long test section, to initiate surface turbulence and create a wind speed profile representing a real-world atmospheric boundary layer (ABL) at the model site (Davenport, 2007).

A combination of low profile surface roughness and spires were used to simulate the length scales of turbulence needed for the atmospheric simulation. To represent a range in the spectrum of turbulence frequencies reported by Davenport (1961) for atmospheric winds, tall spires were used to contribute low frequency spectra while low profile surface blocks were used to contribute to the high frequency spectra. Each wind tunnel has unique requirements of spire and block spacing and geometry to achieve the desired ABL condition. For the spire

design used for this project, the geometric proportions determined by Irwin (1979) were used. Calibration of the spire spacing was then determined during an experimental flow development process to ensure an acceptable level of lateral flow uniformity.

Arrangements of two spire arrays (angles, spacing, location) and surface blocks (spacing and orientation) were tested until successful configurations replicating wind speed profiles for Canadian cities were determined when measured at the location of the leading edge of the urban model. The flow disturbance objects were designed for a 1:300 model scale as described in Section 2.3.

For the wind angles tested, two ABL wind speed profiles were chosen, representing an ABL over open-suburban terrain (OPS) and an ABL over suburban terrain (SUB), typical of the terrain surrounding Canadian cities. Figure 2.1 shows an image of the flow measurement rig consisting of 4 probes mounted on a vertical post covering a vertical distance of 730 mm from the floor. The preliminary ABL flow development test was designed to provide coarse profile measurements useful for identifying significant flow changes caused by changes in the spires and/or block configurations.

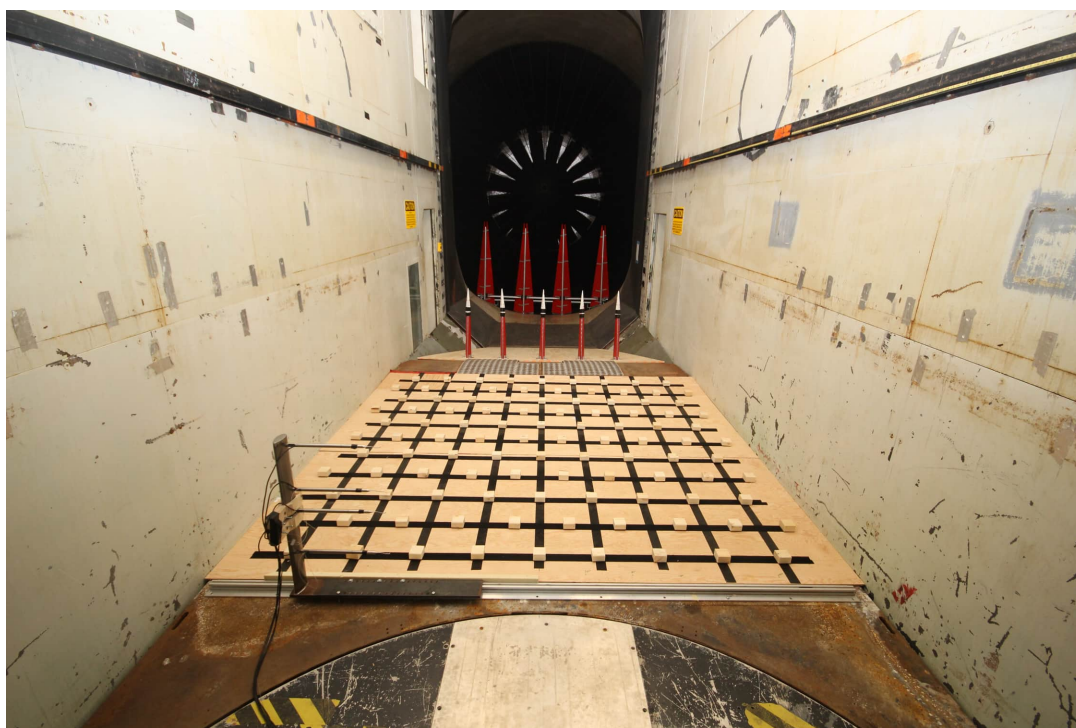


Figure 2.1: Flow conditioning development study test setup.

For the final measurement of the ABL profiles, an automated measurement system designed for the urban airflow measurements, shown in Figure 2.5, was used which enabled higher resolution of the boundary layer profile. Figure 2.2a shows the data point results of the final spire-block combinations for the OPS and SUB wind speed profiles at full scale height, z , along with a theoretical power law curve that is commonly used to represent ABL wind speed gradients.

Figure 2.2b shows the data point results of the final OPS and SUB configurations for the turbulence intensity profile, I_u , defined as:

$$I_u = \sigma_u / U_z \quad (2.1)$$

where σ_u is the streamwise standard deviation of speed fluctuation and U_z is the mean wind speed at the measurement height, z .

The turbulence structures were considered secondary to the wind speed profile because it has been shown by Al Labbad (2021) that the urban canyon flow-field is insensitive to small changes in the upstream turbulence because the wake characteristics caused by the urban structures dominate the inner-city flow-field. The turbulence intensity gradient had a range from approximately 15% at the floor to 7% at the reference height. The range was within the magnitudes measured during full scale field tests reported by Davenport (1961) and was therefore considered sufficient for representing atmospheric wind turbulence for this study.

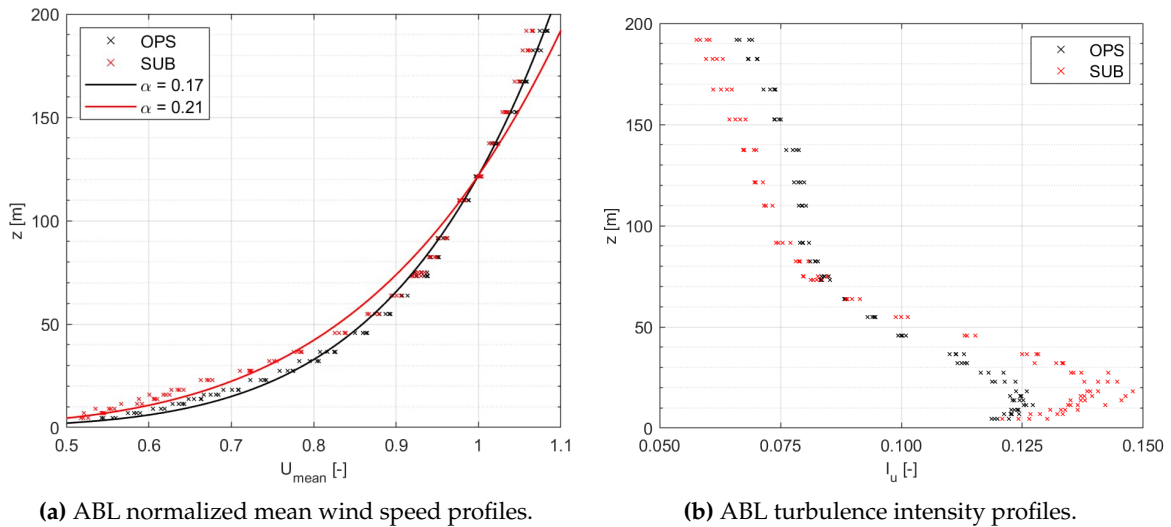


Figure 2.2: OPS and SUB normalized mean flow profiles.

The final spire-block configurations and key dimensions for the ABL profiles and urban flow measurement area are shown in the Figure 2.3 schematic. The illustration shows two sets of spires, an upstream group of four large spires and a downstream group of five small spires. This arrangement was used to improve mixing of the flow and to refine the wind speed profile within the short fetch of the tunnel. All dimensions are shown in millimetres and the distance of the large and small spires from the leading edge of the model are measured in spire heights, where H is the tall spire height and h is the small spire height.

The subtle difference between the OPS and SUB profiles was achieved by orienting the surface roughness blocks differently. For the OPS profile, the blocks were in a low-profile position with frontal dimensions of 38 mm high x 60 mm wide, whereas for the SUB profile, the blocks had frontal dimensions of 60 mm high x 60 mm wide.

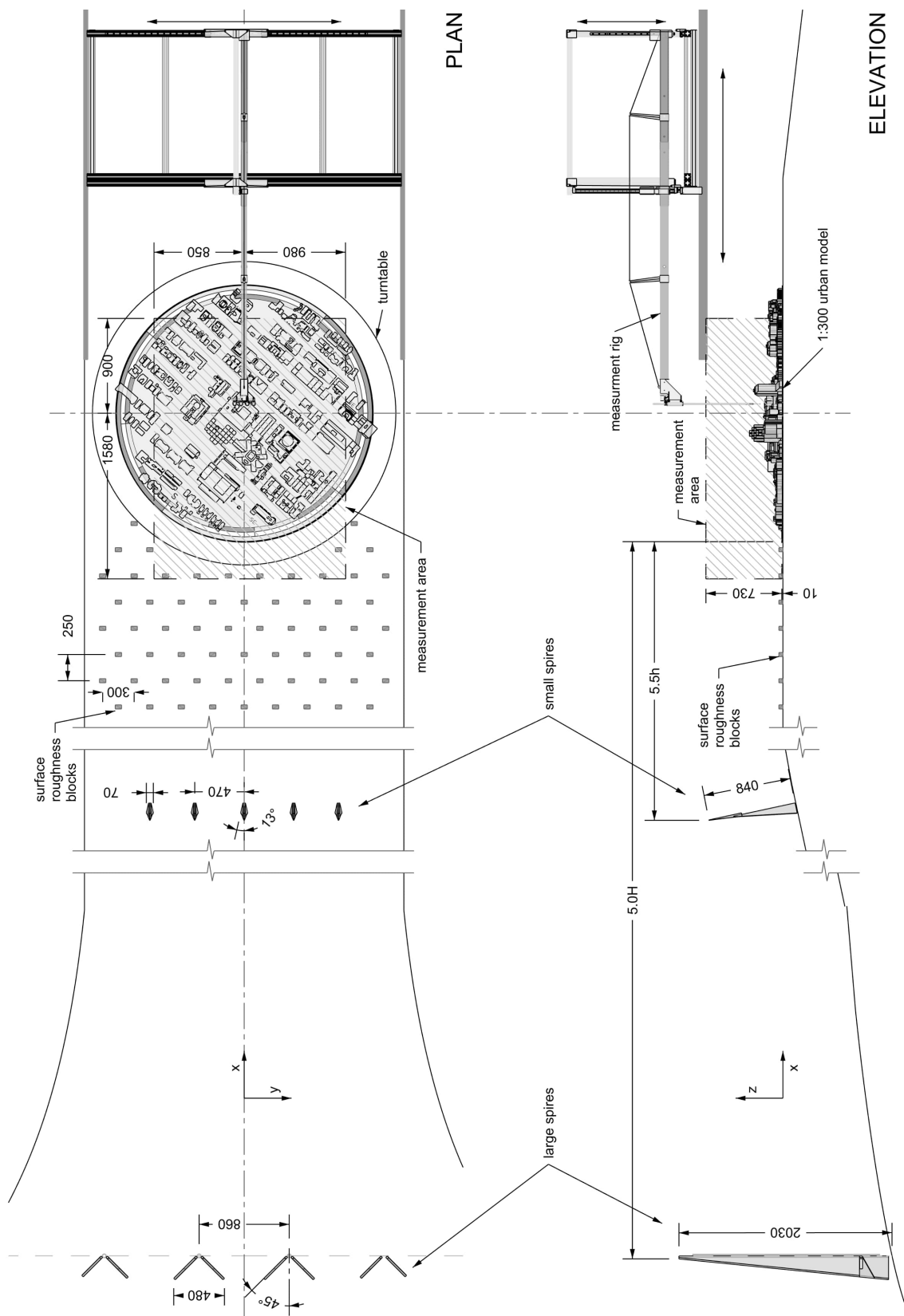


Figure 2.3: Schematic of the wind tunnel setup for urban flow-field measurements.

The reference height for the power law curve was chosen to be 405 mm above the test section floor, which is the model scale equivalent of the regulation altitude limit (122 m or 400 ft) for sRPAS. For the two ABL flow configurations, the wind tunnel fan revolution per minute (RPM) was adjusted to maintain an approximate wind speed of 12 m/s measured at the reference height.

The urban airflow test reference wind speed and model scale were selected to satisfy a Reynolds number (Re) for sub-scale to full scale airflow similitude. The combination of the ABL wind speed profiles and model building sizes resulted in a range of Re within the urban flow-fields. The Re , defined as $\frac{UD}{\nu}$, where U is the wind speed, D is the building width and ν is the kinematic viscosity, was determined to be between 4×10^3 and 10^4 at the reference wind height. For square cylinders with aspect ratio of approximately 1:1, which represent the majority of the urban model buildings, the Re range is within a flow regime where bluff-body wake characteristics are considered consistent (Bai, 2018) and are therefore scalable.

Although the Re varied within the model heights, the reference height was considered a useful region for confirming airflow similitude because it is within the flow-field height that RPAS are expected to fly, and where the flow structures of tall high-rise building wakes will form.

The probe measurements at 405 mm above the test section floor from the OPS and SUB flow conditioning test results were also used to determine the relationship of the pressure drop across the tunnel contraction to the measured wind speed so that during the urban flows testing a calibration curve of the pressure measurements could then be used to determine the mean wind speed at the reference height for normalization of the wind speed results.

2.3 Urban Models

To determine the magnitude of the airflow characteristics that may impact RPAS operation within the urban environment, experimental research was carried out on four urban models representing Canadian cities (Vancouver, Toronto, Halifax, Artificial city). A portion of each real city was selected for a scaled model, representing a building height and density typical of a range in Canadian urban environments.

Scaled models are commonly used to measure wind loads and pedestrian level airflow characteristics of the urban environment (Davenport, 2007; Hertwig *et al.*, 2019). The model scale is typically selected to ensure aerodynamic similitude as noted previously in Section 2.2, but also to accommodate practical constraints. For this urban airflow test campaign, a model scale of 1:300 was chosen to include enough city blocks to simulate an urban flow-field for the wind tunnel turntable diameter while providing adequate space between buildings for the measurement probes.

Three Canadian city replicas and one artificial city were fabricated for the urban airflows testing as shown in the images of Figure 2.4. The three Canadian cities were chosen for features that represent typical types of urban landscapes found in Canada. The features expected to influence the air flowing between and over buildings includes the density of tall buildings, the height heterogeneity of all buildings, building footprint size, street width and topogra-

phy. Although each city model was clearly unique, two similarities were found within all models. Each had isolated tall buildings and groupings of building types, such as hospital campuses. The isolated and grouped buildings provided airflow regions of interest where the speed direction shear turbulence vorticity ($S_1 D S_2 T V$) flow types could be measured across a single-wake and/or within a region of multi-wake interaction.

The Vancouver site is centred on Vancouver General Hospital helipad, rather than the downtown core, to include city blocks where RPAS may be used for medical cargo transfer.

The Artificial City was designed to represent a real Canadian city with additional features to expand the test matrix. The added features represented elements found in Canadian cities that were not fully captured in the other three city models, including a wide central boulevard (modelled after Spadina Avenue in Toronto), buildings with or without balconies, and a modular group of three high-rise buildings that had five possible locations with a range of proximity to one another. Each of the four quadrants of the Artificial City were based on real city blocks taken from various locations within Toronto. The moveable modular group were integrated into each quadrant by replacing existing buildings.

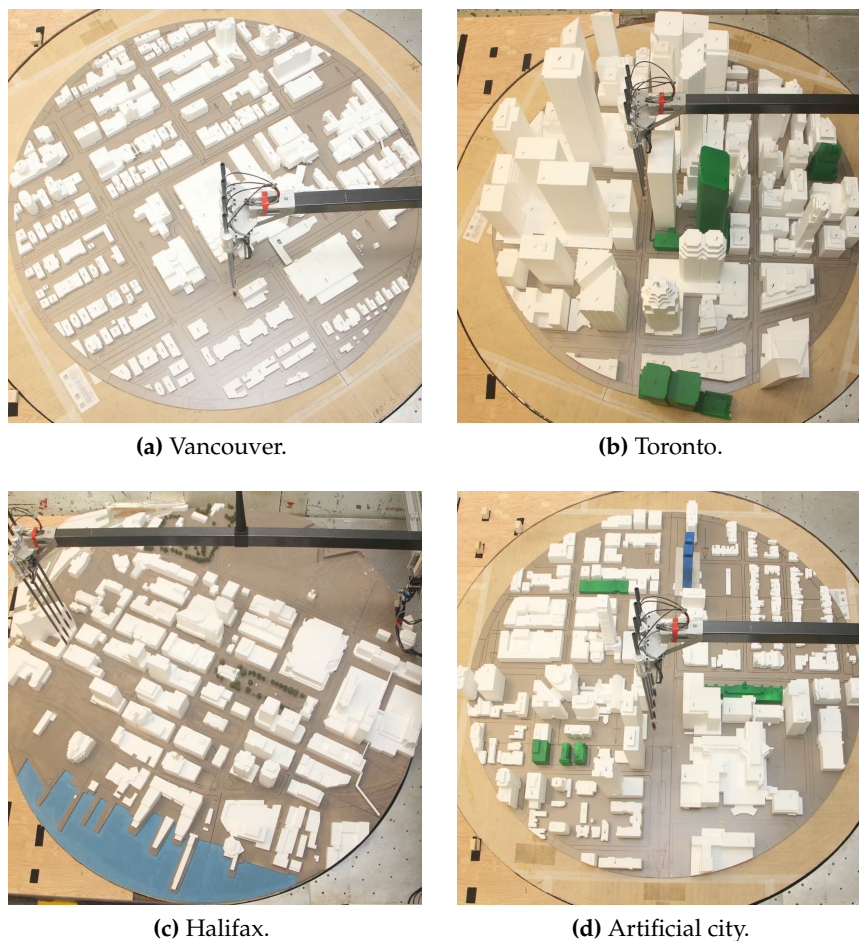


Figure 2.4: Example test configuration for each city model.

The 1:300-scale city models were manufactured by RWDI and comprised of representative foam buildings mounted on 1/8" thick fibre-board. For the Halifax site, which encompassed the peak of Citadel Hill, topography was included as it was considered an important influence on the urban flow-field. The topography created a large step between the test section floor and the model on the Citadel Hill side. Therefore, for wind angles with the hill oriented towards the wind, a multi-piece foam ramp was added to ensure a smooth transition from the test section floor to the height of the model.

2.4 Instrumentation

To measure enough locations within the urban flow-field to compare trends between results for each city model, automation of a multi-probe system was used as shown in Figure 2.5. The system included four probes mounted in a lateral array at a spacing of 60 mm. The spacing was considered far enough apart to prevent flow interference between the probes while providing a useful resolution and enough space that the probe array could safely descend into the street canyons.

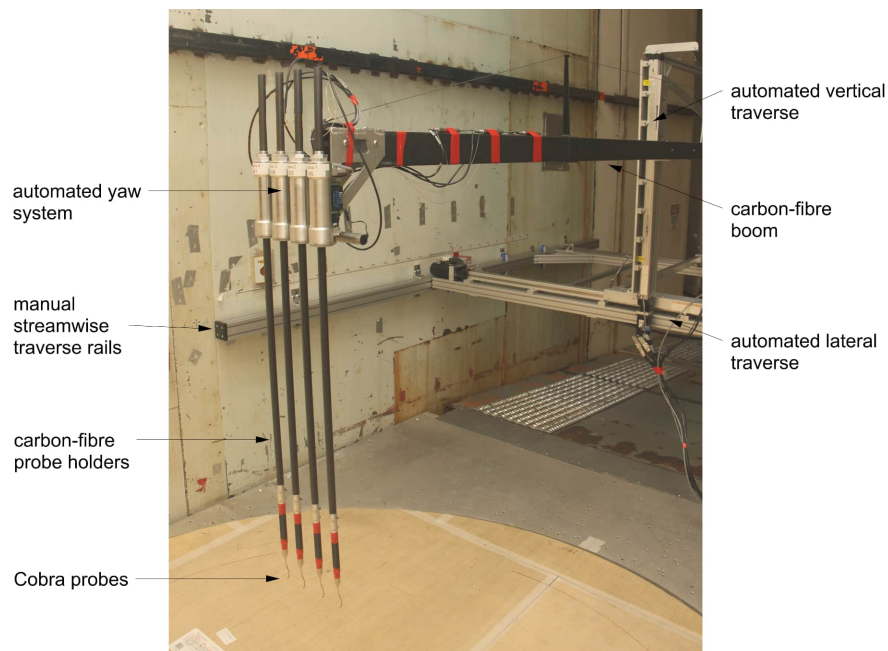


Figure 2.5: Urban airflows measurement system.

Fast-response pressure probes (Turbulent Flow Instrumentation Pty Ltd - Cobra probes) were used to measure the airwake flow characteristics (Hooper and Musgrove, 1997). The data measured by the Cobra probes provide time-series of the three components of velocity and static pressure from which mean values and turbulence quantities were calculated. For the specified velocity range of between 2 m/s and 55 m/s the velocity accuracy is within ± 0.5 m/s and flow angle accuracy within $\pm 1.0^\circ$ (Turbulent Flow Instrumentation, 2022). The Cobra probes have an acceptance cone of $\pm 45^\circ$. Since urban flow includes extreme yaw angles with

respect to the streamwise flow direction an automated synchronized probe yawing system was installed at the probe holder base. The automated yaw system rotated the four probes by up to $\pm 45^\circ$ to orient the acceptance cone to be in closer alignment with the wake flow direction. The automated yawing system was used to repeat a test at a different probe yaw angle after results showed a clear misalignment of the acceptance cone with the wake flow angle.

2.5 Data Processing

2.5.1 Test Conditions

While Cobra probe measurements were being collected, the conditions in the wind tunnel were also being collected. These include:

- The pressure drop across the wind tunnel contraction;
- The temperature and barometric pressure in the test section; and
- The relative humidity as measured outside the wind tunnel.

These quantities are converted to the reference wind speed for each data through the calibration described in Section 2.2.

2.5.2 Cobra Probe Data

During test execution, for the flow measurement data collection, a single run contained the results for a 90 s test case. The data reduction procedures were completed on each run (test case) and each case was stored and analyzed separately. The data reduction process used for this investigation consisted of two steps:

1. Converting the data from the wind tunnel native format into MATLAB time-series data; and
2. Processing, including filtering, applying calibrations, and formatting data as necessary for interpretation.

The tared voltage output signals acquired by the Cobra probes were converted to engineering units using manufacturer-supplied MATLAB library files to provide the following quantities:

- Magnitude, U_{mean} , and orientation (pitch and yaw angles) of the velocity vector;
- Static pressure; and
- The fraction of acquired data points which fell outside the $\pm 45^\circ$ acceptance cone of the probe, also known as the out-of-range (OOR) level.

The fraction of the acquired points that were out-of-range (OOR) was an important characteristic of each data set. Since the probes were often directly in the wakes of buildings, many of the time-series data are subject to significant OOR, which affects the way in which the data is

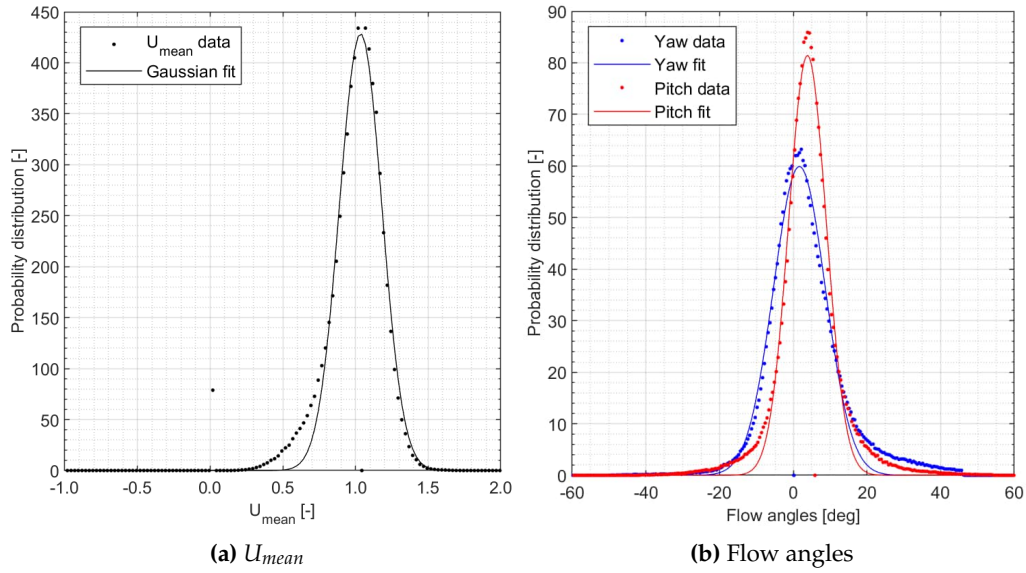


Figure 2.6: Example of probability distribution and Gaussian fit for a data point with 1.2% OOR.

analyzed. Data with OOR rates below 5% are typically considered useable as-is, where larger OOR rates require some care when using the data. Individual measurements falling outside the $\pm 45^\circ$ acceptance cone are known as ‘clipped’ and are given as zero in the final time series. A study of the effect of OOR rate on the yaw and pitch data has revealed ways to recover more accurate mean and standard deviation (std) data depending on whether the turbulence at a given data point is close to normally distributed or not as described by Wall *et al.* (2020).

Basic statistics for each data point were calculated: the mean and std of the flow speed magnitude and flow angles. In every case, these statistics were calculated with the zero time series entries associated with out-of-range data removed. The effect of clipping on the mean is that the mean value may not represent the true mean of the flow speed. The effect of clipping on std is that the value of the clipped signal is always less than the true value.

Turbulence distributions, even in the range of $\pm 45^\circ$, reveal information about the flow characteristics at the measurement point. Figure 2.6 shows a data point with very low OOR (1.2%). The left plots shows the flow speed magnitude and the right plot shows the pitch and yaw angles. The low OOR rate indicated well mixed flow in a far wake or relatively smooth flow region, and the probability distribution is approximately Gaussian.

The mathematical equation for a one-dimensional Gaussian distribution can sometimes be used to recover mean and std by curve-fitting to the data that is available. The Gaussian distribution for a given flow angle β (pitch or yaw) is:

$$\phi(\beta) = \hat{\phi} e^{-(\beta - \bar{\beta})^2 / 2\sigma_\beta^2} \quad (2.2)$$

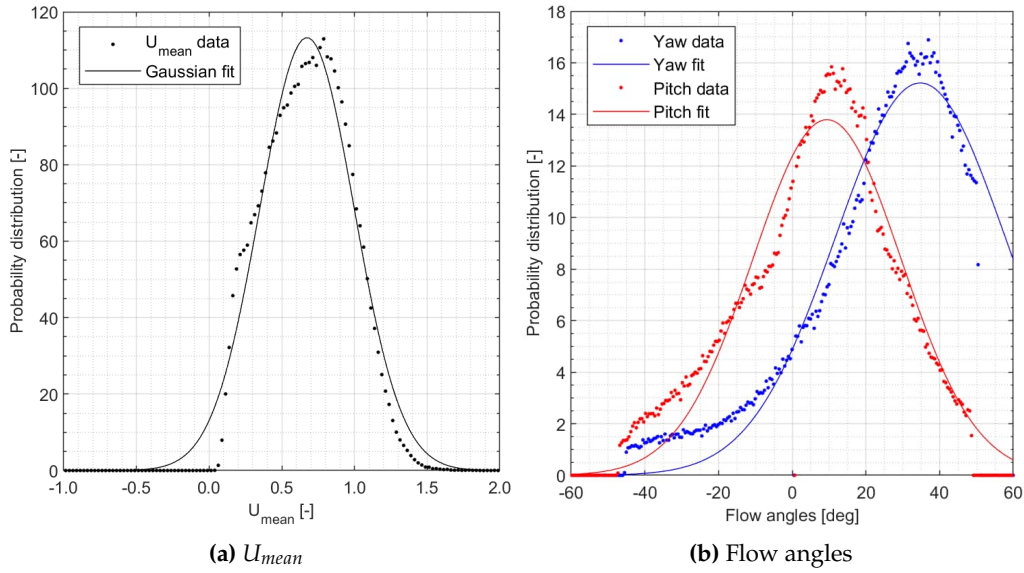


Figure 2.7: Example of probability distribution and Gaussian fit for a data point with 40% OOR.

where,

ϕ is the Gaussian function of the flow angle β ;

β is one of the flow angles;

$\bar{\beta}$ is the fitted mean (centre of the peak);

σ_{β} is the fitted std; and

$\hat{\phi}$ is the magnitude of the peak.

and the Gaussian fitted curves are overlain on the data in Figure 2.6.

For a clipped case, such as shown in Figure 2.7, the overlaid Gaussian fit can be used to extract a signal mean where the mean value of the measured signal does not reflect the true mean. The data shown in Figure 2.7 has an OOR rate of 40%. In the right plot with the flow angles, the clipping is clearly visible in the flow angles, because clipping occurs when the flow angle limit is exceeded. Using Equation 2.2, both the mean and std of the flow yaw data could be recovered for data sets where the data is approximately Gaussian. The mean yaw value of the data set is 22° , where the fitted mean is 35° . The fitted value is clearly more correct, as shown by the image. Clipping is not apparent in the left plot showing flow speed magnitude because clipping affects all instantaneous flow speed magnitudes. For this reason, the mean of the flow speed magnitude can be recovered using a Gaussian fit, but the std cannot. For the data shown in the right image, the calculated mean is 0.66 and the fitted mean is 0.67. In general, the fitted means agree with the calculated means to within a few percent of the reference wind speed, even for OOR rates above 50%.

Since urban flow fields are highly turbulent, a large number of the data points collected had

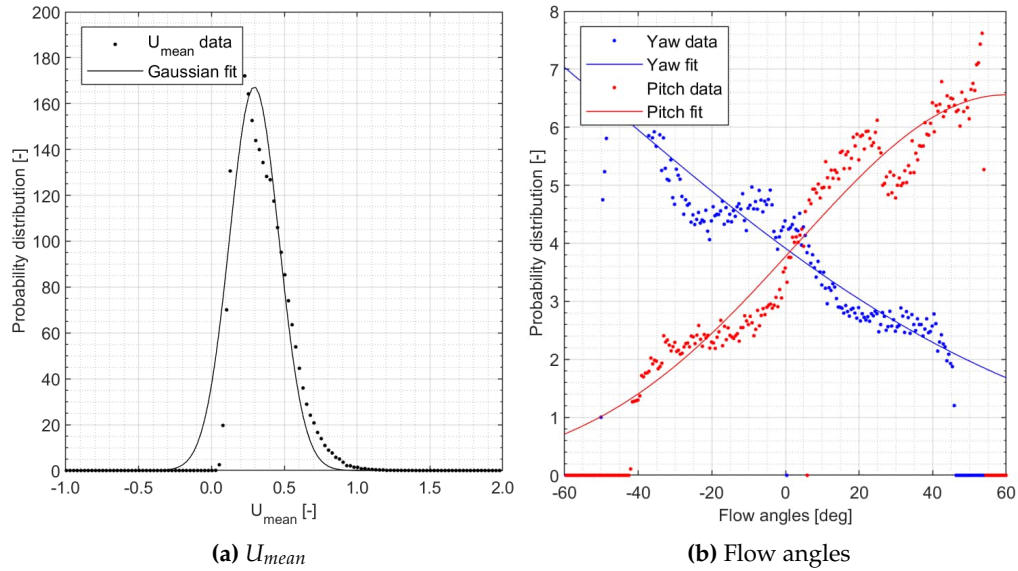


Figure 2.8: Example of probability distribution and Gaussian fit for a data point with 66% OOR.

an OOR rate greater than 5%. For this reason, the recovered magnitude, U_{mean} , was used in the analysis in this report. The calculated std was used, although for high OOR rates, this value is known to under-predict the true turbulence level. Although Gaussian fits enable wider use of the measured data, not all the data collected can be modelled by a Gaussian fit. To avoid the use of erroneous data due to fits, the following criteria for analyzing fitted U_{mean} values were used:

- The recovered mean was not at the end of the data set as shown in the right image of Figure 2.8;
- The Gaussian peak at the recovered mean was not significantly higher (<5) than the original data peak ($\hat{\phi}$) in Equation 2.2; and
- The data did not show a deviation from the overall trend when plotted with nearby data points.

The following criteria were used for analyzing the std values:

- The OOR rate was 50% or less; and
- The data did not show a deviation from the overall trend when plotted with nearby data points.

Some minor errors were found within the Cobra probe data processing code used for the results shown in the mid-year summary report. The results shown in this report may differ slightly from those of the summary report, but no significant changes in magnitudes or conclusions have resulted from the errors.

2.6 Airflow Characterization Program

Measurement planes within the model cities were chosen for a range of wind angles, building wake locations, and possible RPAS flight paths. The characteristics of flow at the measurement planes were expected to capture examples of the flow types identified during Phase I, that may challenge RPAS urban operations, including speed, direction, shear, turbulence and vorticity ($S_1 D S_2 T V$).

The flow-field measurement locations for each city were determined by target regions where extreme $S_1 D S_2 T V$ flow characteristics were expected and by the physical limitations of the probes. Since there was no certainty on where the most extreme flow feature locations would be found, it was critical to cover as many locations as possible. The airflow measured for each city was expected to result in common trends but also to highlight extremes. Therefore the target regions were determined by bluff-body wake characteristics, probable RPAS flight zones, and test plan efficiency for probe manoeuvres.

For each city model, a sequence of location types were used, including:

- A central road intersection (measurement plane: central location (CTR));
- An avenue from a park or parking lot and above the road within the street canyon (measurement plane: avenue location (AVE));
- Downstream of a building with an oblique wind angle where rooftop vortices may form (measurement plane: rooftop vortex location (VOR));
- Downstream of a tall building with a normal wind angle where bluff-body vortex shedding may form (measurement plane: vortex shedding location (SHE));
- A vertical flight path extending from close to the ground to a height where an RPAS may traverse between or over tops of buildings (measurement plane: vertical flight path location (VPA)); and
- A horizontal flight path extending from the top of VPA to another lateral location which represented a reasonable route, such as the hospital helipad for the Vancouver model (measurement plane: horizontal flight path location (HPA)).

For the VPA and HPA test sequences, stationary and moving samples were taken to determine whether a relationship between the moving and stationary measurements can be used to estimate the mean value of the airflow characteristics between discrete measurement points. For the stationary measurements, the mean values were calculated from a 90 s time-series. The moving versus stationary results analysis is not presented in this paper but will be published in a related document in future.

The test sequence started with measurement of the models representing real Canadian cities. The results from those measurements were then used to tailor the test plan for the Artificial city model, to target flow features missing in the real city data set.

For the Artificial city model, additional location types were added to target specific flow features induced by building spacing or details, including:

- An accelerated flow between tall buildings (measurement plane: accelerated flow location (JET));
- The modular building array with a spacing to building width ratio of 0.3:1 (measurement plane: modular building arrangement 1 (MD1));
- The modular building array with a spacing to building width ratio of 0.6:1 (measurement plane: modular building arrangement 2 (MD2));
- The modular building array with a spacing to building width ratio of 0.6:1 with balconies on the upwind and downwind face of the building (measurement plane: modular building arrangement 3 (MD3));
- The modular building array with a spacing to building width ratio of 0.6:1 with balconies on the side-wall faces of the building (measurement plane: modular building arrangement 4 (MD4)); and
- An accelerated flow through a channel at the top of a tall building group (measurement plane: building channel location (CHA)).

Table 2.1 shows the matrix of the wind tunnel test for the Toronto model. The test matrix for Vancouver, Halifax and the Artificial city can be found in Appendix A. In Table 2.1 the nomenclature of each test configuration name is presented in the following format: CITY : WIND-ANGLE : LOCATION TYPE : x-LOCATION : y-LOCATION, where the wind angle represents the clockwise angle from the zero-north datum (270° represents a west wind) and the x- and y-locations denote the centre of the four-probe array in model-scale millimetres. Each test matrix also includes the ABL profile, Cobra probe angle, and full scale (FS) measurement height range.

As previously explained in Section 2.2, the ABL profiles SUB or OPS, denote the flow profile used to represent an upstream wind speed gradient for the type of terrain surrounding each city in the real world environment.

The Cobra probe angle reflects the lateral orientation of the probe, where for 0° , the probe is angled toward the empty tunnel streamwise flow. For some measurement locations, a test was repeated with additional Cobra probe angles when the results showed a high out of range sample indicating flow yaw angles outside of the $\pm 45^\circ$ cone of acceptance of the probe.

The full scale height range of the measurement points is listed on the right of Table 2.1 which is associated with the target airflow type for each configuration. For example, the VPA configurations start at the lowest possible height for the test setup and extend to the height of the HPA, to represent a vertical ascent from ground up to a height where an RPAS may traverse across the cityscape.

Table 2.1: Test matrix: Toronto.

Configuration Name	ABL Profile	Cobra Angle [deg]	Height Range [FS m]
TOR:250:CTR:-170:0	SUB	0	63 - 220
TOR:260:CTR:-170:0	SUB	0	63 - 220
TOR:270:CTR:-170:0	SUB	0	63 - 220
TOR:280:CTR:-170:0	SUB	0	63 - 220
TOR:290:CTR:-170:0	SUB	0	63 - 220
TOR:344:AVE:-180:-630	SUB	0	60 - 135
TOR:344:AVE:-180:-390	SUB	0	60 - 135
TOR:344:AVE:-180:-150	SUB	0	60 - 135
TOR:344:AVE:-180:90	SUB	0	60 - 135
TOR:344:AVE:-180:330	SUB	0	60 - 135
TOR:344:AVE:-180:570	SUB	0	60 - 135
TOR:190:VOR:-450:680	SUB	0, 25	102 - 138
TOR:190:VOR:-450:670	SUB	0, 25	102 - 138
TOR:190:VOR:-450:660	SUB	0, 25	102 - 138
TOR:190:VOR:-450:650	SUB	0, 25	102 - 138
TOR:190:VOR:-450:640	SUB	0, 25	102 - 138
TOR:253:SHE:-300:-240	SUB	-20, 0, 20	180 - 195
TOR:253:SHE:-300:-230	SUB	0	180 - 195
TOR:253:SHE:-300:-220	SUB	0	180 - 195
TOR:253:SHE:-300:-210	SUB	0	180 - 195
TOR:253:SHE:-300:-200	SUB	0	180 - 195
TOR:253:SHE:-300:-190	SUB	0	180 - 195
TOR:253:SHE:-300:-180	SUB	0	180 - 195
TOR:253:SHE:-300:-170	SUB	0	180 - 195
TOR:253:SHE:-300:-160	SUB	0	180 - 195
TOR:253:SHE:-300:-150	SUB	0	180 - 195
TOR:253:SHE:-300:-140	SUB	0	180 - 195
TOR:253:SHE:-300:-130	SUB	-20, 0, 20	180 - 195
TOR:270:VPA:-420:180	SUB	0	33 - 156 ^t
TOR:270:HPA:-257:-60,-300,-540,-780	SUB	0	149
TOR:270:HPA:-257:-60,-300,-540,-780	SUB	0	156 ^t
TOR:270:HPA:-257:-60,-300,-540,-780	SUB	0	164
TOR:270:HPA:-257:-60,-300,-540,-780	SUB	0	171

^t Data collected for stationary and moving probes.

3. Urban Airflow Measurement Results

For the Phase II results, two out of the five flow features from the S_1 D S_2 T V group were analysed, which included speed and turbulence because they were chosen as the first flow types for evaluation of RPAS stability. In part, wind speed was evaluated because sustained wind speed tolerance is the only wind effect specified by the RPAS manufacturers for the tested models. Wind speed was also of primary concern because the wind speed gradient within the urban environment can be more abrupt than for open terrain environments. Turbulence was chosen because it is a commonly accepted influence on flight stability and couples well with speed for wind tunnel testing where hover is the only manoeuvre required to test the failure limits of both flow types.

Following are the urban wind tunnel test results for the speed and turbulence levels measured within the urban flow-fields. For the goals of this urban airflow study, proximity to urban structures is considered directly related to safe RPAS operations. Therefore the results are presented with a focus on the location of the flow feature with respect to distance downstream of a building. This relationship is meant to add a dimension to the analysis which highlights whether a trend in speed and/or turbulence with respect to the distance downstream of a building is evident and/or useful.

3.1 Speed Results

Results for wind speed are presented below in three sections, highlighting the findings as they relate to the urban wind speed characteristics including speed gradient, speed variability and local wind-speed-ratio. Unless otherwise noted, the wind speed is presented as the normalized mean wind speed.

The mean wind speed results were normalized by the empty tunnel mean wind speed determined by a pre-test flow calibration for a height of 405 mm (122 m full scale) above the tunnel floor. Since a standard normalization height does not exist in literature, the normalization height was deliberately chosen to provide a relationship to the full scale sRPAS nominal altitude limit of 122 m (CAR Part IX Section 901.25(1)). This provides a direct reference to the Phase 1 Section 2.2.2 Table 2.1 of Barber and Wall (2020) which describes a method for estimating the urban wind speed gradient relative to the atmospheric boundary layer wind speed at 122 m above ground.

3.1.1 Speed Gradient

Figures 3.1a to 3.1d show the results of the normalized mean wind speed, U_{mean} , for all data points for each city model. The data points for the simulated atmospheric boundary layer (ABL) flow, measured at the leading edge of the city model, are included on the left-hand side of each figure to provide a comparison of the urban flow results to the approaching flow.

The urban flow results, in the main part of each image, are presented with respect to the horizontal distance to the nearest upstream building shown on the x-axis. If there was no upstream building for the wind angle, and the flow path was clear from the ABL measurement location to the data point measurement location, the data point is plotted on the right hand side of the plot at a distance of 750 m (labelled “no upstream building”). All of the data points are denoted by a coloured marker, which maps the measurement height to the colour bar legend shown to the right of the plots. The green markers denote heights within a low-rise building height (< 24 m), the cyan markers denote heights between a low-rise and the altitude limit for small RPAS (122 m) and the red markers denote all heights above 122 m. All distances, are plotted in full scale metres.

In comparison to the ABL U_{mean} gradient, which increases monotonically with height, the urban flow results show mixing of the U_{mean} values for the range of heights for each city, and a reduction in U_{mean} for a large portion of the data points. In general, U_{mean} values as low as 0.1 were found for all city models including for locations with an upstream building and without an upstream building, where the flow was slowed by the interaction of the building wakes.

The maximum U_{mean} values for all city models were above 1.0 for heights in red, at or above 122 m, and without upstream buildings. For Halifax and Vancouver, the result was not unexpected because the tallest buildings were around 100 m, but for the Artificial city and Toronto the tall high-rise wake interaction could have reduced the wind speed. The results indicate that the low density of the high-rise buildings is porous enough for the ABL wind speed at 122 m to prevail into the urban core at some locations. This finding is significant because it identifies that the U_{mean} value used to normalize the results, persisted into the urban environment. This supports the rule of thumb described in the Phase I report Figure 2.2 of Barber and Wall (2020) that estimates that the open terrain wind speed at 122 m can be transferred to the urban environment for Canadian cities.

A correlation between height and wind speed is somewhat evident within the results for Vancouver, where the green markers are clustered below the cyan markers, but not for any of the other cities. In particular, the results for Toronto show a consistent mix of red and cyan markers for the full range in U_{mean} . Although some regions may exist within the city models where the vertical gradient of the ABL persists, within the measured data set the absence of a height-to-speed correlation suggests that rather than following a progressive trend, the vertical gradient can be considered variable.

3.1.2 Variation in Wind Speed

Examples of variation between the ABL wind speed gradient and the urban flow measurements for all city model results is evident by the mix of colours throughout the test results shown in Figures 3.1a to 3.1d. Extreme examples of the variation can be seen in the plots for Toronto and the Artificial city.

Within the Toronto plot, Figure 3.1b, several red markers are below a U_{mean} of 0.2 including for points with and without the presence of an upstream building. Considering the red markers are located at a minimum of 122 m above ground, it can be concluded that the wind speed at

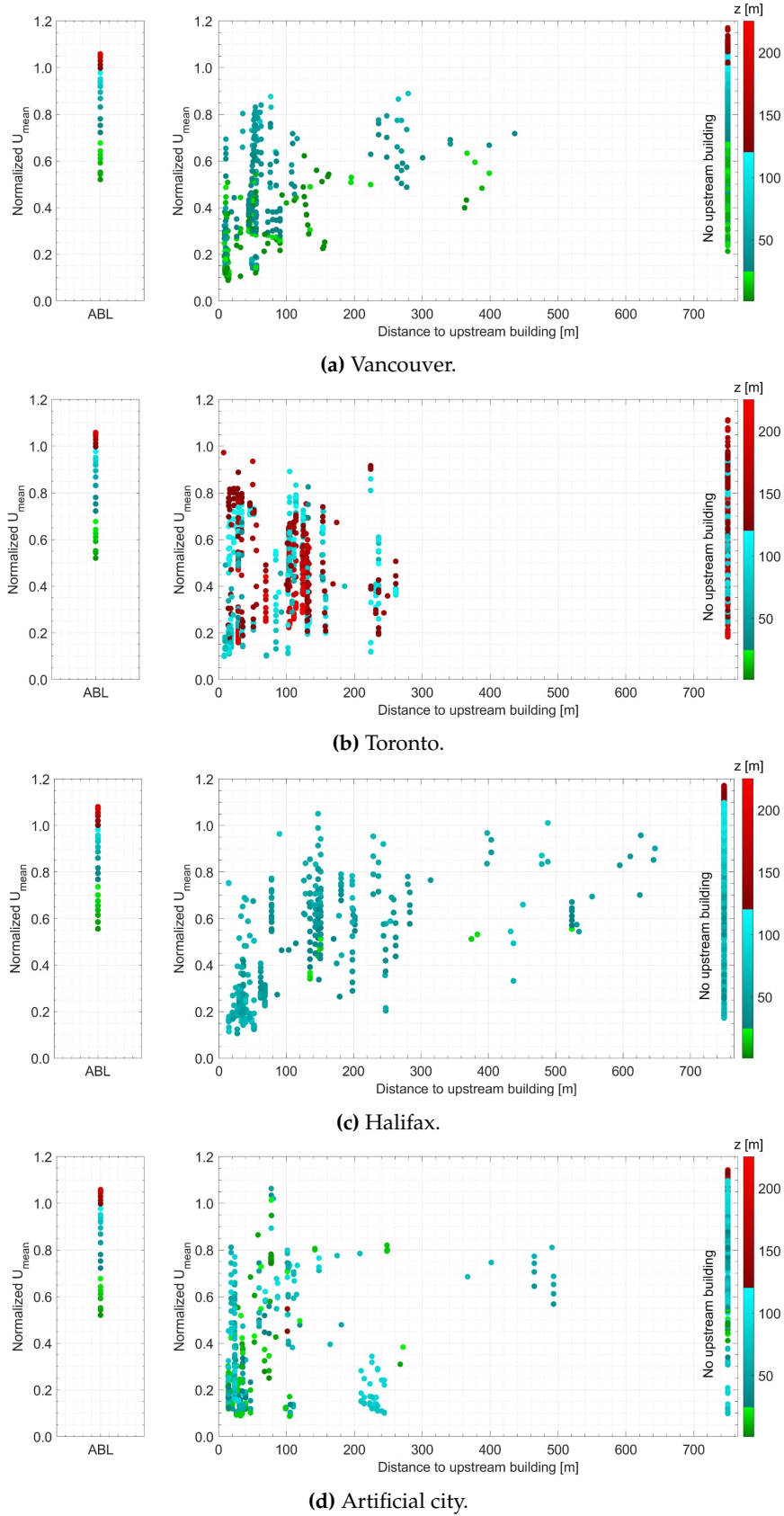
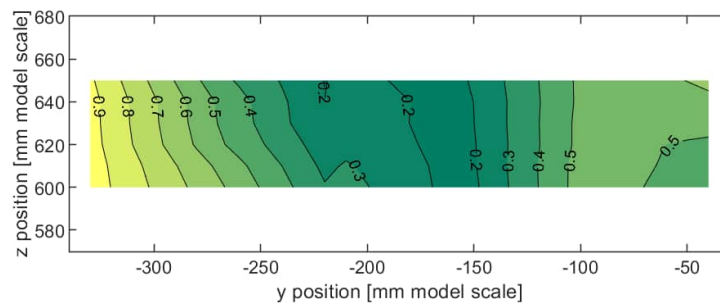


Figure 3.1: Experimental results of normalized mean wind speed, U_{mean} .

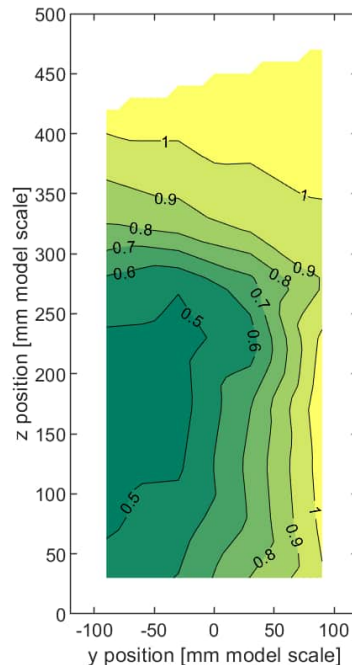
that height has been reduced by over 80% (from over 1.0 to 0.2), for a streamwise distance between the ABL measurement location to the city location.

Alternately, an increase in wind speed can be seen within the results for the Artificial city, where a green marker is present above a U_{mean} of 1.0. In this case, for the green marker which represents a height low to the ground (< 24 m), the wind speed has accelerated to exceed the ABL wind speed at that height by over 50% (from 0.68 to 1.03).

Both of the highlighted cases of extreme variation are shown in contour plots in Figure 3.2, where the y and z axis show the measurement plane location in model scale and the contours represent the U_{mean} results. The case nomenclature noted in the figure caption identifies the city, wind angle and location, where Figure 3.2a shows a Toronto model (TOR) with a west-southwest wind angle of 253° at a location specifically chosen to find bluff body shedding (SHE) as defined in Section 2.6.



(a) Normalized U_{mean} contours showing decreased speed at high height. Case: TOR-253-SHE.



(b) Normalized U_{mean} contours showing increased speed at low height. Case: ART-315-CTR.

Figure 3.2: Cases of extreme urban flow mean wind speed variation.

The contours show the large variation over a short distance and that the U_{mean} gradient is not always vertical, and can be lateral as a result of building wake shear layers. These cases demonstrate an extreme shift in flow characteristics from the upstream ABL flow to the location of the urban flow measurement.

3.1.3 Local Wind-speed-ratio

The acceleration, defined as a local increase in flow speed, of airflow within the city is described in the Phase I video and report Section 2.2.6 of Barber and Wall (2020) as a “venturi effect” and is described as urban airflow that increases in speed in comparison to the freestream wind speed. Results from the urban flows test showed that the extreme changes in wind speed within the urban flow-field were primarily a result of the slowing of wind speed within the near-wake of a building rather than as a result of the speed-up within a constricted flow path. Therefore, rather than observing small increases in wind speed with respect to the freestream, local wind-speed-ratio was analysed to observe extreme changes over short distances within the urban flow-fields. Large changes in wind speeds over small distances are an indicator of a challenging RPAS environment.

Figure 3.3 compares the ratio of U_{mean} between adjacent measurement points in the lateral plane. Assuming that a flight path could traverse in either direction, passing through accelerating or decelerating wind speeds, the results are presented as absolute ratios, where the result is always greater than 1. The measurement spacing for the urban flows testing was typically set to the probe array spacing of 60 mm (18 m full scale). For some tests, where a finer increment was needed to measure details of flow structures, 20 mm (6 m full scale) and 10 mm (3 m full scale) increments were measured. Figure 3.3 shows results of the adjacent point U_{mean} ratios, with the blue markers denoting 60 mm spacing, the magenta markers denoting 20 mm spacing, and the black markers denoting 10 mm spacing.

For each city, results are presented with respect to height, z , to demonstrate the effect of a decrease in building density on the results. For all of the city model results, the majority of the data points have an adjacent point U_{mean} ratio of between 1 and 2. For Toronto, a more consistent spread of data points between 1 and 2 are found for a larger range in height, as expected by the blockage of flow from the taller high-rise buildings.

For all city models, the most extreme ratios had a range from 2 to 5.4 and every city demonstrated a ratio greater than 2.6 over a lateral distance of 18 m. A particularly notable wind speed ratio was observed in Vancouver, where a wind speed ratio of 3 was observed over a lateral distance of 6 m which is approximately 6 to 20 body lengths of common sRPAS. This location is downstream of a tall narrow building, where one of the adjacent measurement locations is inside of the near-wake recirculation zone and the other is outside of the recirculation zone, within the shear layers.

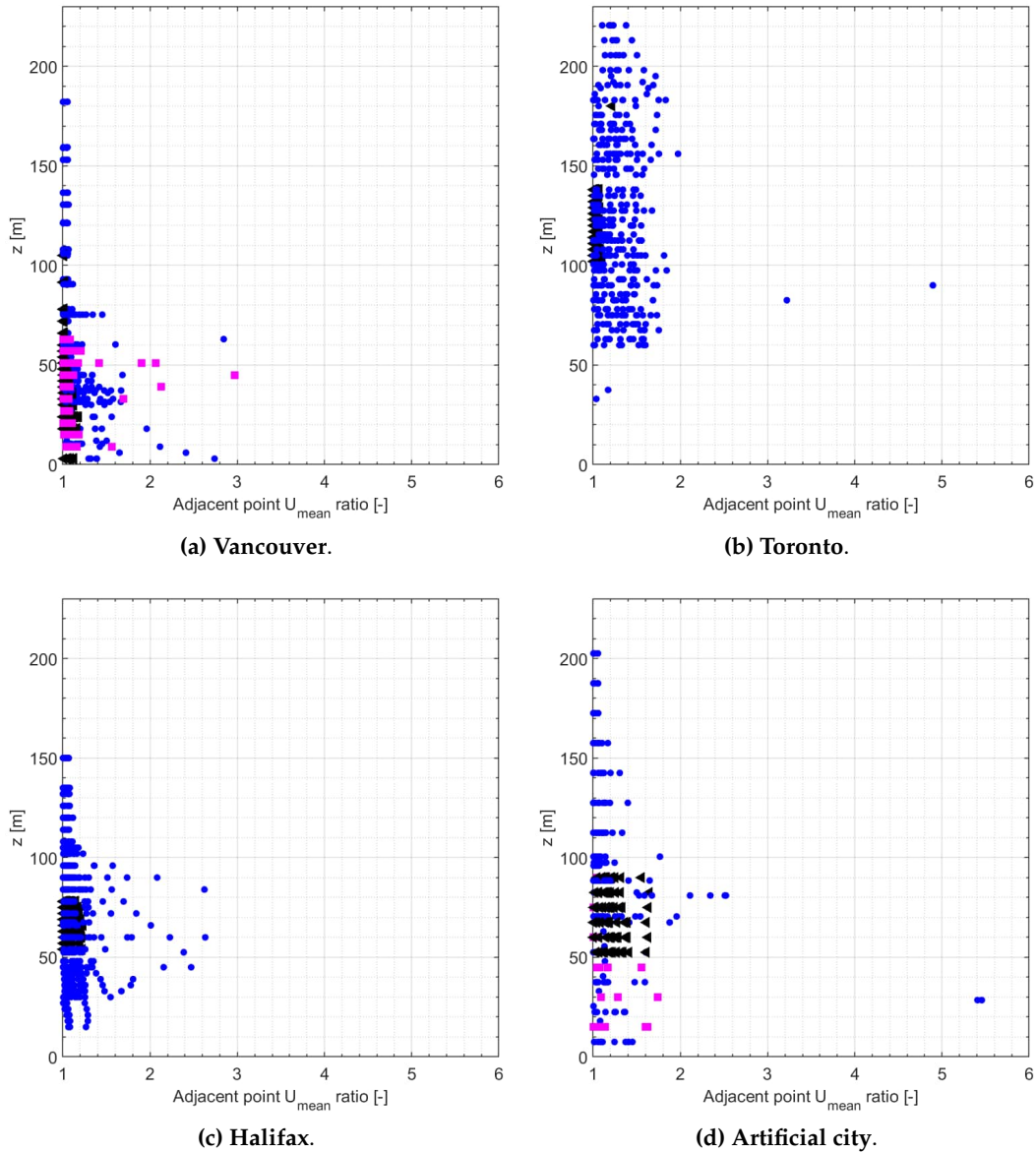
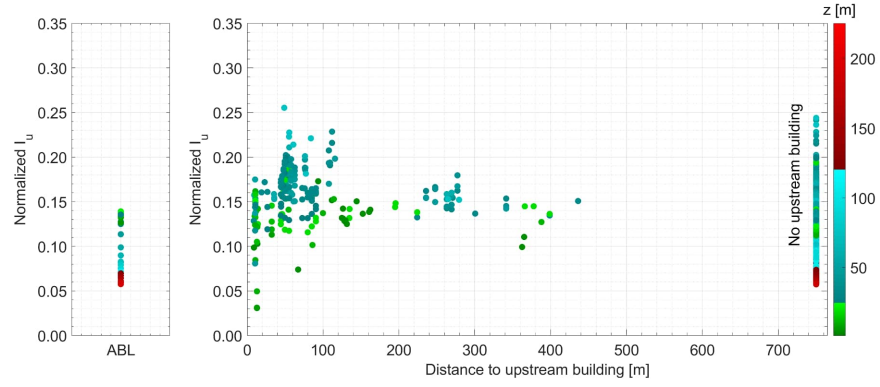


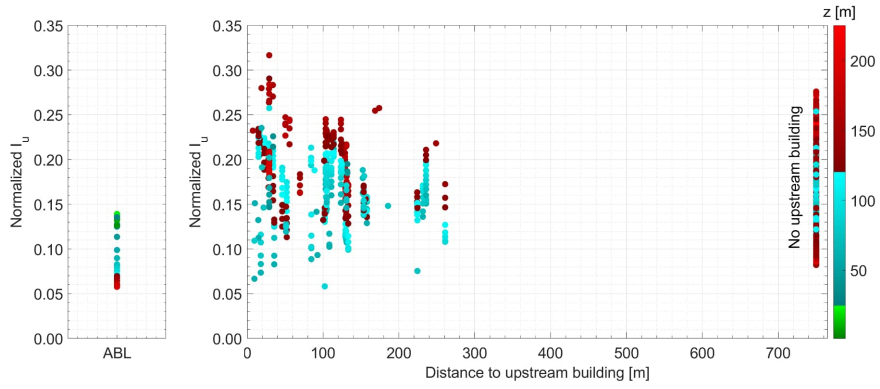
Figure 3.3: Experimental results of local wind-speed-ratio within the urban environment.

3.2 Turbulence Intensity Results

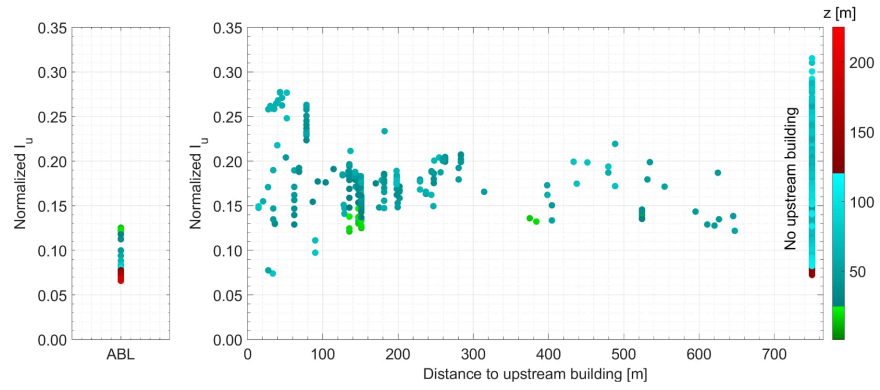
Within the building wakes, the slowing of the flow is caused by the conversion of smooth currents into turbulent eddy structures. The reduction of wind speed is therefore expected to relate to an increase in turbulence intensity. Figure 3.4 shows the turbulence intensity plotted using the same layout and coloured height mapping as for the U_{mean} plots, where results for turbulence intensity, I_u , were determined by dividing the standard deviation by the local mean wind speed for each data point time-series.



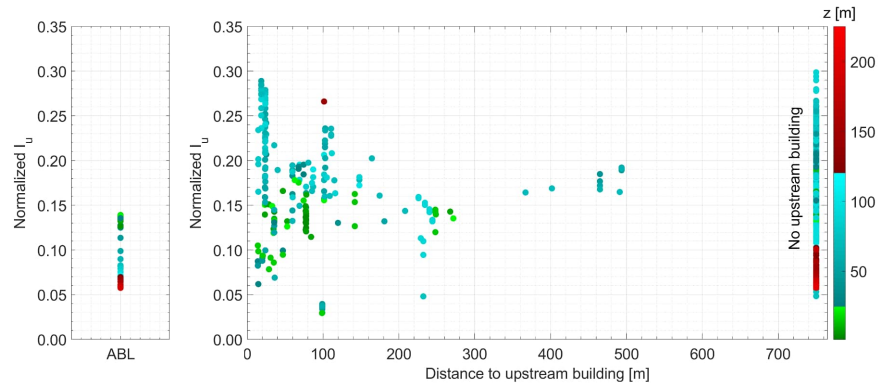
(a) Vancouver.



(b) Toronto.



(c) Halifax.



(d) Artificial city.

Figure 3.4: Experimental results of turbulence intensity, I_u .

In general, the results for all cities show an increase in I_u with a decrease in proximity to an upstream building. The high I_u values for locations with no upstream building are expected to be a result of turbulent building wakes, which permeate into the street canyons. Table 3.1 lists the maximum values of I_u for each city along with the U_{mean} and height, z , for that data point. U_{mean} is included to examine the magnitude that U_{mean} has decreased at the location of the highest measured I_u .

Table 3.1: Maximum results for I_u .

City	I_u [-]	U_{mean} [-]	z [m]	z [ft]
Vancouver	0.26	0.71	75	246
Toronto	0.33	0.82	164	536
Halifax	0.32	0.60	90	295
Artificial	0.30	0.65	89	290

The results show that for the maximum I_u locations, where I_u ranges from 26% to 33%, the U_{mean} has a range from 60% to 82%. The combination of the high wind speed and the height range (relative to each model) indicate that the location of maximum I_u is found above low-rise buildings and within the higher roughness region of the urban flow-field. Figures 3.5 to 3.8 show the location of data points within the city models for each of the test configurations associated with the maximum I_u values. A contour plot of the I_u results for the test cases is shown over the data points (red markers), with the location for the maximum value highlighted by a black circle. For some data point locations, the contour plot colours do not fill the entire rectangular measurement plane. This is a result of the omission of the over 50% out-of-range data as explained in Section 2.5. The I_u at the data point locations within the missing contours is likely higher than the noted maximum value, due to the highly turbulent nature of the flow causing the high OOR.

To demonstrate the probable origin of the turbulent wake flow, the plan view in the figures includes a cross-section plane B-B, at the height of maximum measured I_u , except for Halifax, where the height of the measurement plane was above all buildings. Similarly, the elevation view shows the cross-section plane A-A, which cuts through the measurement plane, showing the proximity and density of adjacent buildings. The plan view is oriented with the section plane A-A perpendicular to the flow for the purpose of relating the plan view to the elevation view. The wind angle arrow, labelled U_∞ is shown to highlight the oncoming wind orientation.

The location of the maximum I_u data point for Toronto is between tall high-rise buildings at 164 m above ground and 30 m downstream of a building corner at building mid-height as shown in Figure 3.5. This measurement plane, HPA, was chosen as a potential height for an RPAS flight path because it is above most of the buildings and has large enough gaps between the buildings at that height, for clear passage. For a 270° west wind angle, a flight through this measurement plane location would include areas of significantly high turbulence. The changing intensity of the turbulence is associated with the building wakes and, as seen on the left side of the contour plot, with the rooftop wake recirculation region.

Figure 3.6 shows the location for the Vancouver result which is above the hospital helipad. The dark line below the contour plot is the cross-section through the hospital helipad. For the 160° wind angle, the landing is within the wake of a tall building, causing a non-uniform flow-field across the width of the helipad landing plane within the height of the tall building. At the

height of the high-rise building, the I_u changes from 16% to 26% in 15 m, vertically downward. For an sRPAS, which can descend at around 5 m/s, therefore the pilot would have to react to a 60% increase in turbulence within 3 s while flying through a high wind speed ($U_{mean} = 0.71$).

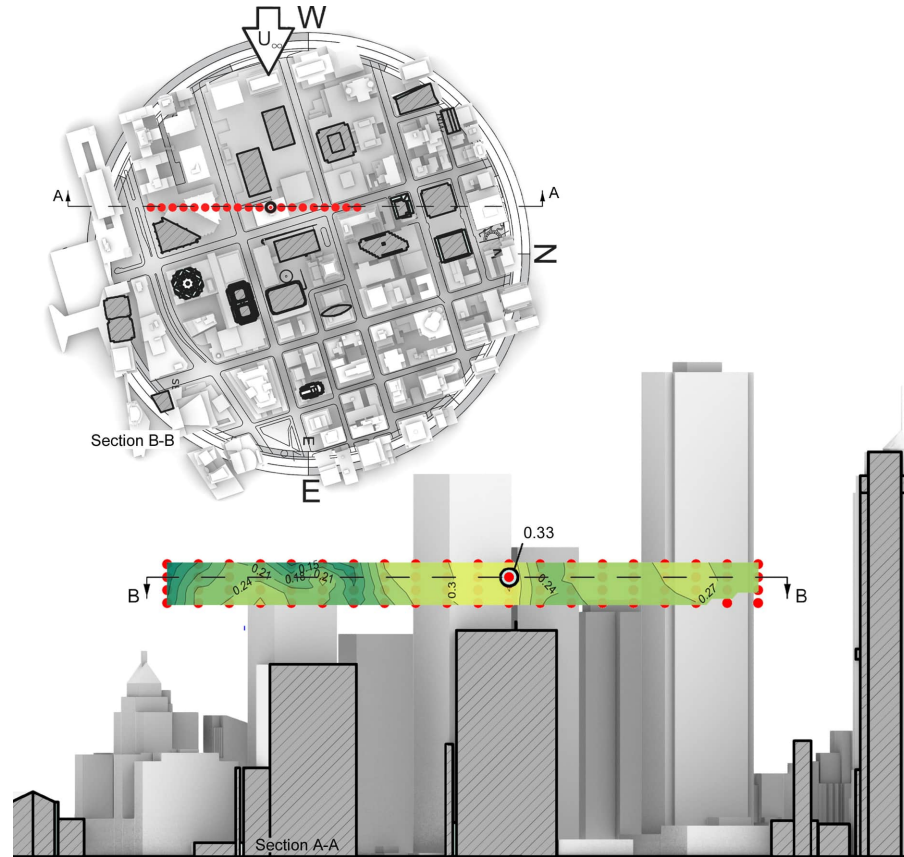


Figure 3.5: Location of extreme I_u for Toronto, case: TOR:270:HPA.

For the other two cities, the location of the maximum I_u is downstream of a building, with the rooftop recirculation region. These cases demonstrate the intensity of turbulence in the rooftop wake. For the Halifax results shown in Figure 3.7, the upstream building is large and isolated although it is part of the downtown core. The shape of the turbulence intensity contours suggest that the higher turbulence is emanating from the wake of the raised architectural piece at the rooftop, which is 6 m tall x 16 m wide. The corner of the architectural detail is 6 m away laterally and 80 m upstream of the measurement location.

For the Artificial city, the extreme I_u is shown for a location above a group of buildings representing an array of three high-rise buildings (86 m), with a spacing-to-building width ratio of 0.6:1, replicating closely spaced high-rise buildings in Toronto. For this test configuration, the buildings upstream of the high-rise are all low- to mid-rise buildings, with heights well below that of the modular group (<34 m). The contour plot results show a core of high I_u at the top right corner of the outer building. A larger region with 26% I_u can be seen across the central part of the measurement plane from mid-building height extending upward to include the

rooftop wake. The measurement plane was 15 m FS downstream of the buildings and within the wake recirculation region where the flow is diverting in different directions. The size and shape of the 26% contour suggests that a portion of the wake has become a multi-building wake where the I_u is consistent for a larger region than for a single building wake.

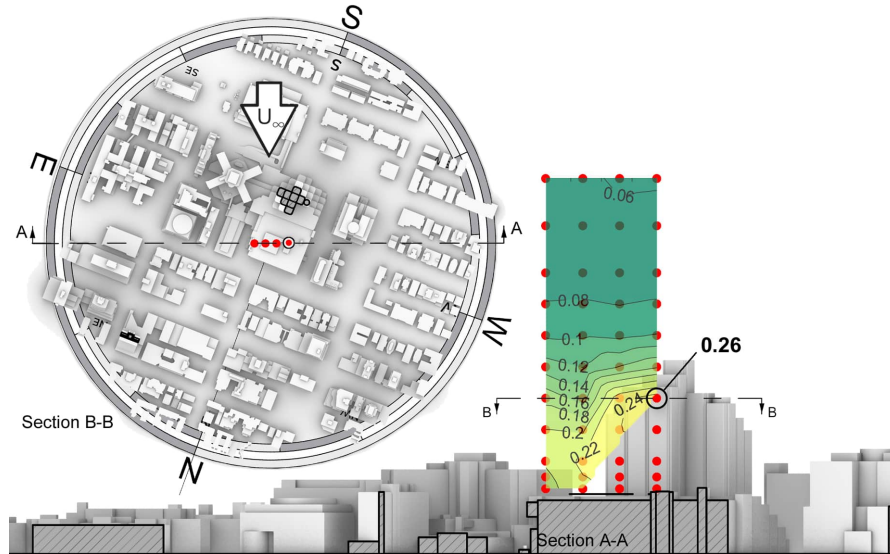


Figure 3.6: Location of extreme I_u for Vancouver, case: VAN:160:CTR.

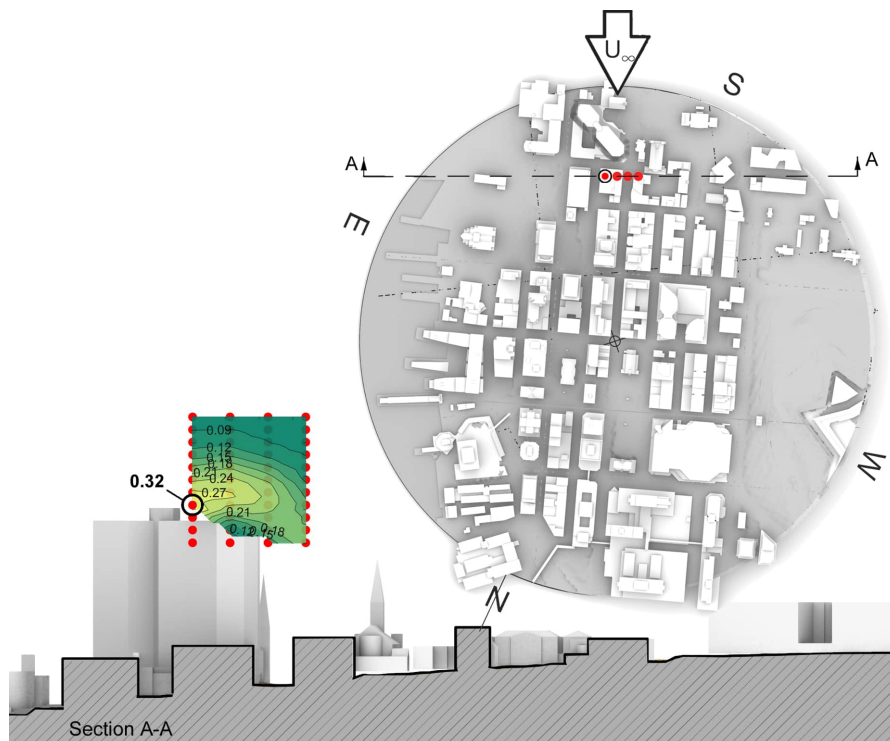


Figure 3.7: Location of extreme I_u for Halifax, case: HAL:155:SHE.

The results for Halifax and the Artificial city demonstrate that regions of high turbulence can come from the wakes of small building features and large building groups, where the frontal area of the structure(s) determine the cross-section size of the wake. The comparison of the results for Halifax and the Artificial city also show that the wind angle affects the flow angularity of the wake, where the Halifax rooftop wake, induced by a wind-to-building face flow attack angle of 40° , has a bulge of high I_u extending towards the right of the contour plot. The Artificial city multi-building wake, which has a perpendicular wind angle, has a I_u pattern that is centred on the building group.

From Figures 3.5 to 3.8 it is evident that the proximity to a building is the dominant factor for determining where the highest region of I_u will exist, but that the wind angle and grouping density and/or size define the pattern and lateral location of the high I_u region.

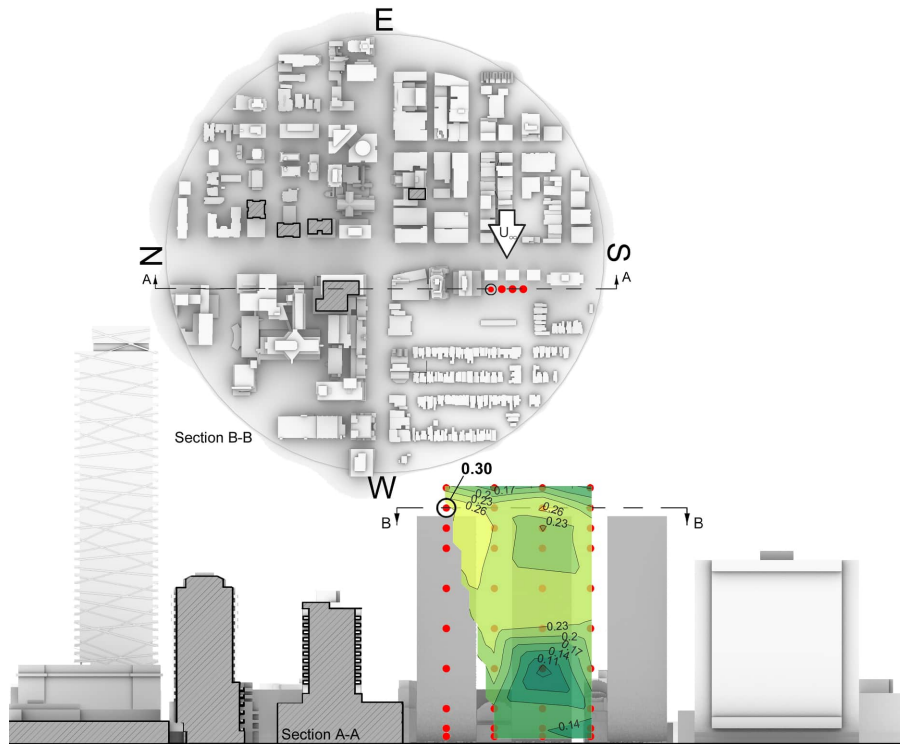


Figure 3.8: Location of extreme I_u for the Artificial city, case: ART:90:MD2.

Although extreme values of I_u are of most interest, the locally-averaged values help to understand the relationship of the measured I_u with height above ground and narrow the area of focus for finding the extremes. From Table 3.2, which compares the average I_u and corresponding height for each height group, it is evident that the I_u is also dependent on height.

For all cities with measurements within the height of a low-rise building (green), the average I_u is approximately 13% for a height above ground of between 12 m and 20 m.

For the results from measurement heights between low-rise rooftop height and 122 m (cyan), the average I_u is approximately 15% for a height between 62 m and 87 m. Interestingly, al-

though the cities have a range in building height and heterogeneity, the average turbulence intensity within the cyan height range is consistent, even when compared to the results for Toronto, which has high-rise buildings above 122 m and the other city models do not.

For the results from measurement heights above 122 m (red) a large contrast was found between the city models, with Toronto having the highest average of all heights, at 20%, whereas the other three city model results have the lowest result because the measurement height is above the buildings. The right-hand column of Table 3.2 shows the typical height of the tall buildings for each model. When comparing the typical tall building height to the average I_u values for each city, the results show a positive correlation between height and I_u within the roughness boundary layer of the cities, but above that height the I_u drops back to freestream levels.

Table 3.2: Average I_u results for each urban height reference colour in Figure 3.4.

height range:	Green		Cyan		Red		
City	\bar{I}_u [-]	\bar{z} [m]	\bar{I}_u [-]	\bar{z} [m]	\bar{I}_u [-]	\bar{z} [m]	Typical tall building height [m]
Vancouver	0.137	15	0.140	62	0.066	156	80
Toronto	n/a	n/a	0.157	87	0.201	159	240
Halifax	0.135	20	0.150	76	0.089	129	80
Artificial	0.125	12	0.156	71	0.088	165	90

Although this report presents the results for wind speed and turbulence intensity in separate plots to highlight overall trends for each flow characteristic, results were found for all city models where both the wind speed and the turbulence intensity was high (approximately 1.0 and 0.15 respectively). This finding suggests that the highly turbulent airflow regions in a city are not limited to low wind speed wake regions, but can be present with high wind speed. The variation of wind speed with turbulence levels may be a significant area of study for determining challenging RPAS operations in the urban environment.

4. Testing of Small RPAS

Specifications provided by manufactures of small RPAS (sRPAS) typically include a sustained wind speed tolerance (SWT). The specification documentation does not reveal the method used to determine the limit or whether the wind speed includes atmospheric turbulence. For this first phase of wind tunnel testing of RPAS for wind speed and turbulence in urban airflows the purpose of the testing was to evaluate the specified sustained wind speed tolerance for each RPAS model in hover position for a variation in airflow turbulence intensity and to observe the reaction of the RPAS stability to turbulence levels found during the Part 1 urban airflows testing. Additional wind tunnel RPAS manoeuvres were added to the test program to evaluate whether the wind limits for the RPAS were also dependent on RPA orientation or traversing into turbulence.

In this report stability refers to the behaviour of the aircraft including the autonomous parts of the stabilizing system but not the pilot. Therefore, the wind speed tolerance was determined by the wind speed at which the auto-pilot was no longer able to maintain position, and the pilot was required to add control. This method assumes that the RPAS is being tested independent of the pilot's skill level and the pilot workload. Future testing may include RPAS operator workload and skill level effects, but for this initial test, the primary variable was RPAS stability limits.

The test setup and procedures were tailored for a range in sRPAS size with turbulence flow conditions representing intensity levels measured within the flow-fields of the Part 1 urban airflow study. This chapter and Chapter 5 include details of the RPAS test program, presents results and conclusions and a summary with future objectives.

Similarly to the urban flows testing, the RPAS wind tunnel test program was carried out at the 3 m × 6 m Wind Tunnel in Ottawa, Canada. Since the facility was suitable for testing of sRPAS for the selected flow types it was cost effective and practical to use the same facility for the Part 2 testing. The test program included measurement of the smooth and turbulent airflow conditions, testing of four sRPAS by TC pilots and testing of one sRPAS by SME IndroRobotics.

The following sections describe the wind tunnel flow conditioning system, turbulent flow results, RPAS-models and -settings, data collection system and the data processing.

4.1 Flow Conditioning for Turbulence Intensity

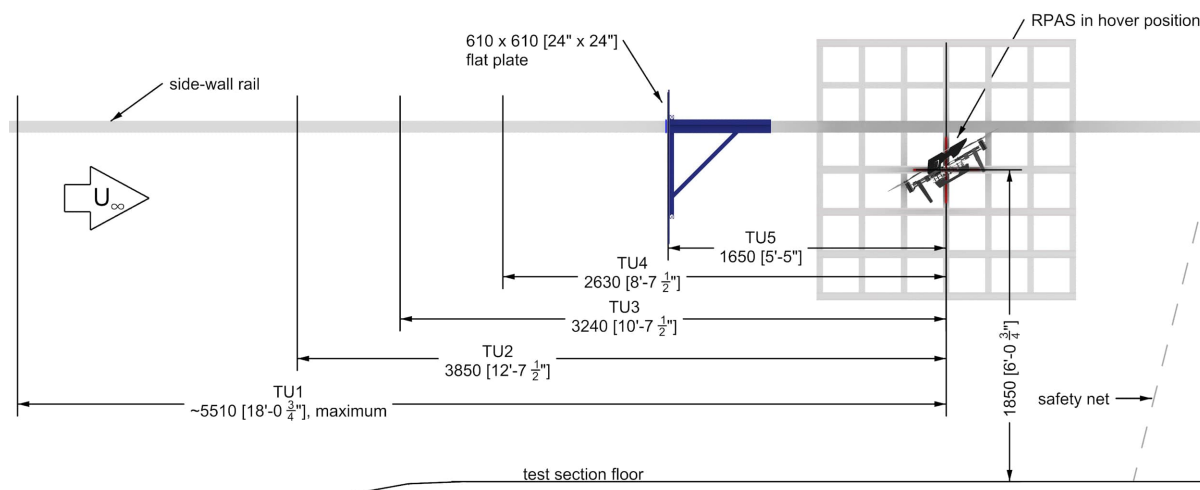
To control the wind tunnel airflow for smooth and turbulent conditions a portion of the test section was used for a turbulence generating system. The system comprised of a 19 mm thick plywood plate mounted, at lateral centre, to a tunnel cross-brace frame that slides along the test section side-wall channels. The turbulence intensity was controlled by moving the cross-frame closer or further from the nominal hover position, allowing for quick transition between test configurations.

Figure 4.1 shows an image of the turbulence generator in the wind tunnel with the flow survey rig at the hover position and illustrates an elevation of the test section setup including the locations of the turbulence generator, nominal hover position, and the downstream safety net.

The turbulence intensity generated by the flat plate was also dependent on the cross-section size of the plywood. The 610 mm x 610 mm plate was designed to provide a turbulence intensity range from 10% to 20% as estimated by the conclusions from a previous study by Nedić *et al.* (2013) on near wake characteristics downstream of flat plates in normal flow.



(a) Turbulence generator set up for flow survey.



(b) Turbulence generator location schematic.

Figure 4.1: Cases of extreme urban flow mean wind speed variation.

The dominant length scale generated by the shedding frequency of the flat plate were on the order of magnitude of the plate cross-section, ranging from approximately 0.6 m to 0.8 m for the wind speed range of 5 m/s to 20 m/s. This size of fluctuating flow was expected to challenge the sRPAS stability by applying an oscillating component of a similar length scale to the sRPAS overall size.

The wind speed and turbulence intensity were evaluated for each of the turbulence generator locations (TU1, TU2, TU3, TU4, TU5) at wind speeds of 5, 10, 15 and 20 m/s for a 90 s interval. Due to instability in the measurement rig at the higher turbulence configurations, the TU3 and TU4 measurements did not include 20 m/s.

The turbulent wake flow survey measured a cross-sectional plane of the airflow at the hover location using the Cobra probes described in Section 2.4 mounted in a re-configured array. The vertical spacing between probes was 250 mm and the lateral measurement locations were taken from -750 mm to 750 mm in increments of 250 mm. An example of the turbulence intensity, I_u , results for TU4 for a wind speed of 15 m/s is shown in Figure 4.2, where the overall range of the plot on the y-axis represents the overall width of the tunnel. Since the turbulence intensity created by the wake of the flat plate had a gradient, decreasing outward from the wake core, the turbulence intensity was identified as the value measured at a diameter of approximately 1 m centred on the hover position. Since the overall size of all tested RPAS models was within 1 m, it was assumed that the flow condition turbulence intensity was at the measured level during the RPAS test.

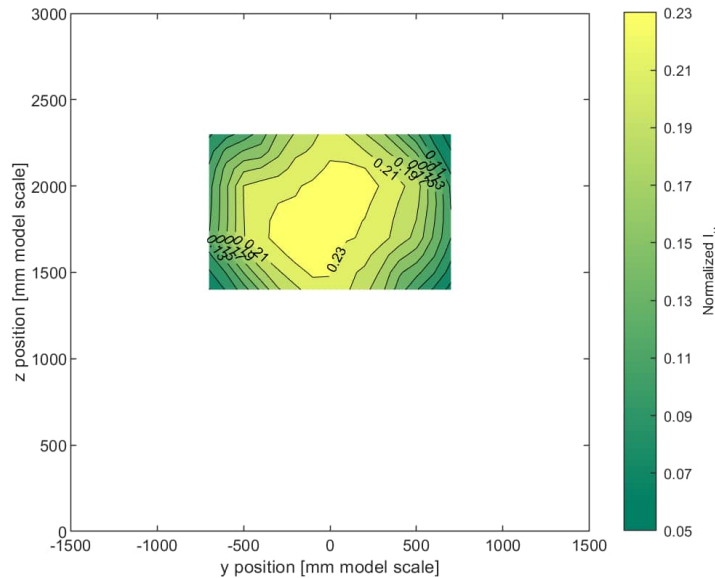


Figure 4.2: TU4 turbulence intensity contour plot results measured for a wind speed of 15 m/s.

The turbulence flow mapping found only minor variations in turbulence intensity at 5 m/s of $\pm 1\%$ for TU1 and TU2, but a consistent turbulence intensity for all other wind speeds and TU locations. The stability of the turbulence intensity for the range in wind speeds allowed for flow configurations for the sRPAS testing where wind speed was incremented for a known turbulence intensity with each generator location.

Figure 4.3 shows the results of the turbulence intensity, I_u , measured at the RPAS hover location with a wake core wind speed of 10 m/s, for the five turbulence generator positions. In the plot, the downstream distance from the plate to the measurement plane, x , is multiplied by the square root of the frontal area, A .

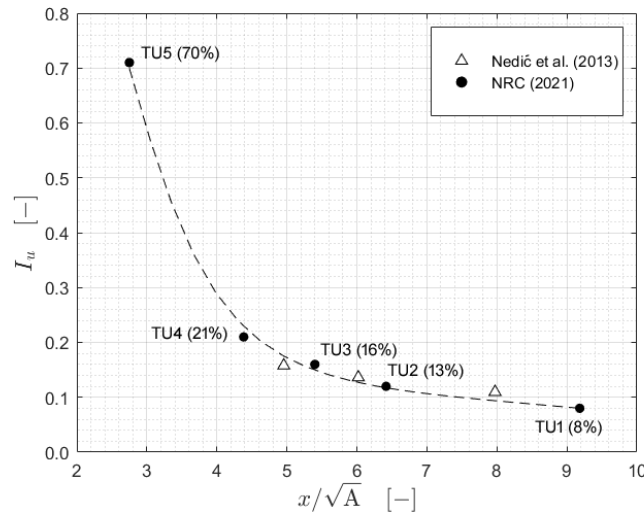


Figure 4.3: Turbulence generator results for five downstream locations. Nedić *et al.* (2013): Δ ; NRC (TU1 - TU5): \bullet .

Although the results for the Part 1 urban airflow characterization found that the extreme turbulence intensities were on the order of 30%, the RPAS testing started with I_u as low as 8% (TU1) to expand the test matrix to evaluate a trend and to ease the pilot towards the higher I_u levels.

In relation to the urban environment, the range in turbulence intensity level from TU1 to TU5, when compared to the urban airflow characterization could be considered representative of:

- 8% atmospheric turbulence which may occur above the building rooftop wakes, or within areas of stagnated flow within the urban canopy, such as within the centre of a recirculation zone just downstream of a large building. The perimeter of the recirculation zone will be no larger than the building width and can range in height from close to the ground to close to the rooftop (Kuznetsov *et al.*, 2016).
- 13% to 16% turbulence regions which may occur within building wakes for a large range of distances from a building, but outside of the core of strong building wake features such as rooftop vortices, rooftop shear layers or side-wall shear layers.
- 21% turbulence regions which may occur within the core of building wakes above rooftops for all wind angles or at the extreme gradients coming from shear layers at the sides of buildings when the wind is normal to the building face. This level of turbulence can be present from within a few metres to over 100 m within the wake of a building.
- 70% turbulence regions may occur in the smaller wakes of small objects. Although this level of turbulence does not represent any cases from measurements taken for the urban

airflow characterization, it does represent turbulence caused by winds normal to a structure at a location approximately 1.5 m downstream if the structure has a size similar to the turbulence generator panel. The size is relative to small rooftop structures such as vents, rectangular chimneys, air-conditioning units or solar panels.

4.2 RPAS Models and Flight Settings

Four DJI RPAS were tested by TC RPAS pilot certificate holders (Mavic Mini, Phantom 4 Pro, Mavic 2 Zoom, and Matrice 300) and an Autel EVO Dual II Pro was tested by a professional SME pilot (IndroRobotics). Quadcopters like these are typically used by hobbyists and professionals for activities that suit rural and urban operations such as sport flying or surveillance. The range in weight was from 0.249 kg to 6.3 kg. Therefore all but the smallest, the Mavic Mini, fit within the weight category specified by Part IX of the Canadian Aviation Regulations (CARs) for sRPAS, which require registration and incident reporting. Figure 4.4 shows images of the five RPAS models during testing in headwind orientation. A visual line of sight of the RPA was kept by the pilot at all times from a viewing station outside of the wind tunnel and above the hover area. The RPA control settings and sensors typically used for navigation were limited during the tests due to the indoor test section environment, where there is no GPS reception. Therefore, the RPAS visual positioning systems were the only automated positioning system used. To improve the response of the visual positioning systems, the tunnel environment was enhanced using high contrast grids on the floor and wall.

Flying in the wind tunnel was also a challenge for the pilots as a result of the RPAS detection systems and the closeness of the tunnel walls and safety net. The preferred mode and detection settings for each RPAS that was critical for safe flight within the confines of the wind tunnel are listed in Table 4.1.

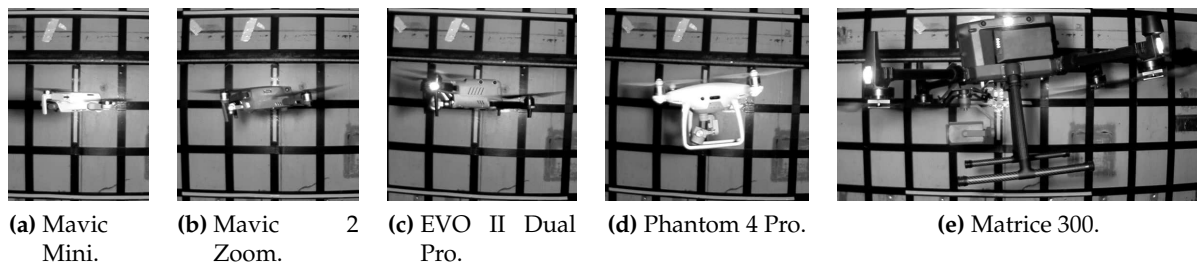


Figure 4.4: Wind tunnel test: RPAS models in headwind orientation, with wind coming from the left side.

4.3 RPAS Flight Procedures

The test flight procedures were designed to evaluate the wind speed limit, or U_{mean} limit, for each RPAS while limiting damage to the RPA from repeated loss of control incidents. For each

Table 4.1: RPAS wind tunnel flight settings.

RPAS Model	Setting
Mavic Mini	Cine Mode
Mavic 2 Zoom	Horizontal detection OFF, Tripod Mode
Autel EVO II Dual Pro	Object avoidance OFF, Normal Mode
Phantom 4 Pro*	Horizontal detection OFF, Tripod Mode
Matrice 300	Horizontal detection OFF, Upward object detection ON, Tripod Mode

* due to the metal construction of the testing facility, compass error occurred inside the test section, compass calibration was attempted outside and inside of the test section without success. The number of tests were minimized for this model operating without compass calibration which required more pilot input.

test, the initial wind speed was slow, enabling the pilot to establish stable hover. As the wind was increased, the pilot intervened as needed to reposition the RPA. When the RPA was then maintaining position the pilot allowed the auto-pilot to take over while data was collected. If the RPA could not maintain a position without pilot interference the test was stopped and the failure limit was reached. At the failure wind speed, the wind tunnel fan was stopped at either the pilot's request or upon collision with the net. The U_{mean} limit was identified when the RPAS instability required the pilot to override the auto-pilot to maintain course during data collection.

Testing for wind speed and turbulence was done in a headwind and a cross-wind hover position. The test configurations for a headwind orientation included:

- An incremented wind speed gradient without turbulence;
- A continuous wind speed gradient without turbulence;
- An incremented wind speed gradient with turbulence;
- A continuous wind speed gradient with turbulence; and
- A vertical traverse into turbulence with incremental increases in wind speed between each traverse.

The test configurations for a cross-wind orientation included:

- An incremented wind speed gradient without turbulence; and
- An incremented wind speed gradient with turbulence.

For the incremented gradient (incr) tests, the wind speed was increased in steps of 1 m/s. Each wind speed test included a 30 s data collection. For the continuous wind speed gradient (cont) test, the acceleration of the wind tunnel flow was increased at the maximum rate of 0.95 m/s². The duration of data collection for this type of test included the entire wind speed sweep and the U_{mean} limit was determined for the wind speed at which the RPA slipped downstream past the end of the side-wall grid.

The headwind vertical traversing manoeuvre included a hover above the turbulent wake, a

descent into the hover location, a stabilization period, a 30 s data recording and then if the wind speed limit was not reached, an ascent back to the initial position above the turbulence.

4.4 Data Collection System and Post Processing

Three data collection systems were used to compile results including video recordings from a wall-mounted camera viewing the hover location, video recordings from the onboard RPAS camera, and RPAS log files when available. The RPAS camera was directed towards the tunnel floor to capture the RPA position and information that was projected onto the test section floor including tunnel wind speed, time, and test configuration. A frame from a recording from each system is shown in Figure 4.5. The video recordings were used to verify notes taken during each test to determine the wind speed at which the auto-pilot could no longer maintain position and the RPAS log files were used to observe RPAS variables in time-series format.

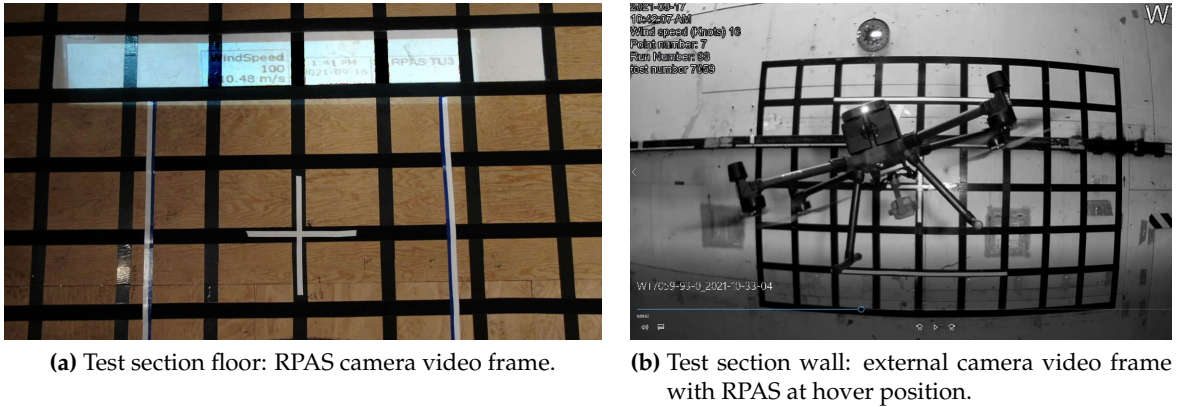


Figure 4.5: Wind tunnel video recording examples.

The RPAS log files were used to evaluate the variation in the RPA attitude angle by converting the time-series of the individual motor speeds into ratios for the pitch and roll configurations of the RPAS system (Burggräf *et al.*, n.d.) as follows:

$$\text{Pitch motor ratio} = \left(\frac{FR + FL - BR - BL}{FR + FL + BR + BL} \right) \quad (4.1)$$

$$\text{Roll motor ratio} = \left(\frac{FR - FL + BR - BL}{FR + FL + BR + BL} \right) \quad (4.2)$$

where FR, FL, BR, BL are the front right, front left, back right and back left motor speeds, respectively. The time-series of the motor ratio was then used to compare variation between tests.

For this first RPAS wind tunnel test, live observations along with the video recordings were useful for cross referencing when determining the U_{mean} limit. For more detailed evaluation of specific performance characteristics or pilot actions, the RPAS log files are required. The RPAS log files contain detailed RPAS time-series information that has not been fully analysed, but for this study, were useful for evaluation of the effect on RPAS performance due to airflow turbulence.

5. Small RPAS Test Matrix and Results

The wind tunnel test matrix and the results are shown together in the following section to provide a single reference table for comparison of test range and results of each RPAS model. Not all RPAS were tested for each flow configuration due to elevated risk of damage for particular tests and/or model types. Table 5.1 shows the test program matrix with results for the measured sustained wind speed limit, or $U_{mean} \text{ limit}$, listed in the right-hand column. The $U_{mean} \text{ limit}$ has been shown in bold text for the values that are below the manufacturer's specified sustained wind speed tolerance (SWT).

In general, the test matrix evolved during testing in reaction to the pilot's comfort with flying each type of RPAS in the wind tunnel environment. The testing of the Autel EVO II and the DJI Phantom 4 was limited to lower-risk incremental tests after visual observations of highly unstable reaction of the RPAS to turbulent flow.

Loss of control occurred in one of two ways, a slow slip in the direction of the wind and a fast spontaneous shift in position and orientation sometimes resulting in a collision. The reasons for the spontaneous failures are uncertain, but likely related to the testing environment or the RPAS detection settings including the positioning system which may not have provided adequate flight stability under the flow circumstances. Only four spontaneous failure cases are included in the results, for cases where a clear wind speed limit was found immediately before the loss of control. The number of wind speed limit results from the loss of control due to windward slip show a clear relationship of test condition to the auto-pilot control limit and therefore the cases that may include failure due to the test environment, such as lack of GPS signal, are considered insignificant with respect to the reported results.

When compared to the manufacturers specifications for sustained wind speed tolerance, the results from the smooth and turbulent flow condition wind tunnel tests showed inconsistency between manufacturers. The testing indicated that all RPAS had a higher $U_{mean} \text{ limit}$ than the manufacturer's SWT tolerance when flying in smooth flow, except for the Autel EVO. For the other RPAS, the SWT was reached for one of the levels of turbulence intensity. This discrepancy indicates that a standard method for evaluating sRPAS for wind conditions is not consistent within the industry.

For all sRPAS models, the TU5 turbulence intensity of 70% was considered too high for safe operation. Although that level of I_u is not representative of the urban flow-field measurement results from Part 1, where the measurement locations were centred on street corridors, it could represent turbulence levels closer to urban structures. Since the Mavic Mini was resilient to collision with the tunnel boundaries and had the lowest replacement cost it was briefly tested with the TU5 configuration. The result was inconclusive because although the wind speed was at the lowest tunnel speed of 4 m/s, spontaneous loss of control of the RPAS occurred during ascent through the turbulent wake shear layers before the pilot could ascend into the hover position.

Table 5.1: RPAS wind tunnel test matrix and results.

RPAS Tag	RPAS Model	SWT [m/s]	Flow-Orientation -Test Type	Flight Manoeuvre [m/s]	I_u [%]	U_{mean} Range [m/s]	U_{mean} limit [m/s]
A	DJI Mavic Mini	8.0	SMT-0-incr	Headwind Hover	0.5	4 - 13	12.5
			TU1-0-incr	"	8	4 - 12	11.1
			TU2-0-incr	"	13	4 - 11	10.3
			TU3-0-incr	"	16	4 - 10	9.1
			TU4-0-incr	"	21	4 - 8	7.6
			TU5-0-incr	"	70	4	-
			SMT-90-incr	Cross-wind Hover	0.5	4-8	7.0
			TU3-90-incr	"	16	4-8	7.2
			SMT-0-cont	Headwind Hover	0.5	0 - 10	9.6
			SMT-0-cont	"	0.5	0 - 10	9.6
			TU3-0-cont	"	16	0 - 13	12.9
			TU3-0-trav	Vertical Descent/Ascent	"	4 - 10	8.6
			TU4-0-trav	"	21	4 - 8	7.5
B	DJI Mavic 2 Zoom	10.6	SMT-0-incr	Headwind Hover	0.5	4 - 16	15.8
			TU1-0-incr	"	8	4 - 15	14.9
			TU2-0-incr	"	13	4 - 14	12.2
			TU3-0-incr	"	16	4 - 12	11.7
			TU4-0-incr	"	21	4-11	9.8
			SMT-90-incr	Cross-wind Hover	0.5	4-18	17.9
			TU3-90-incr	"	16	4-12	12.1
			SMT-0-cont	Headwind Hover	0.5	0 - 16	15.9
			SMT-0-cont	"	0.5	0 - 20	15.9
			TU3-0-cont	"	16	0 - 16	12.7
			TU3-0-trav	Vertical Descent/Ascent	16	4 - 15	14.9
			TU4-0-trav	"	21	8 - 13	10.8
C	Autel EVO II Dual Pro	21.0	SMT-0-incr	Headwind Hover	0.5	9 - 16	15.9
			TU3-0-incr	Headwind Hover	16	7 - 12	8.6
			TU4-0-incr	"	21	6 - 10	9.0
			SMT-90-incr	Cross-wind Hover	0.5	9 - 12, 12.5	12.2
			TU3-90-incr	"	16	6 - 10	*
			TU3-0-trav	Vertical Descent/Ascent	16	7 - 10	8.6**
D	DJI Phantom 4 Pro	10.0	SMT-0-incr	Headwind Hover	0.5	4 - 15	13.6
			TU3-0-incr	"	16	4 - 12	10.9
			TU4-0-incr	"	21	4 - 12	7.0
E	DJI Matrice 300	15.0	SMT-0-incr	Headwind Hover	0.5	7 - 19	19.0
			TU1-0-incr	"	8	7 - 16	15.8
			TU2-0-incr	"	13	7 - 17	15.8
			TU3-0-incr	"	16	7 - 13	12.7
			TU3-0-incr	"	16	10 - 15	14.8
			TU4-0-incr	"	21	7-12	11.8
			SMT-90-incr	Cross-wind Hover	0.5	10-19	19.8
			TU3-90-incr	"	16	7-16	16.1
			SMT-0-cont	Headwind Hover	0.5	0 - 19	18.9
			SMT-0-cont	"	0.5	0 - 20	19.8
			TU3-0-trav	Vertical Descent/Ascent	16	4 - 15	14.7
			TU4-0-trav	"	21	7 - 15	13.9

* drifting towards net at each wind speed, pilot intervention required, no result.

** failed in smooth flow above turbulent wake after completing the test for the noted speed.

U_{mean} limit result in **bold** indicates that it is less than SWT.

For the turbulent flow configurations, the smaller DJI drones reached a U_{mean} limit lower than their respective SWT when I_u was 21% (TU4), whereas the larger Matrice 300 reached a U_{mean} limit lower than the SWT at an I_u of 16% (TU3).

The test results for the traversing manoeuvre show that the RPAS U_{mean} limit was not affected by crossing between smooth and turbulent flow. However, a significant and consistent change in RPAS position occurred for this type of test. When the RPAS transitioned into the turbulent wake, the RPAS lunged upstream as a result of the reduction in flow wind speed. For real-world application, this suggests that crossing into a building wake in close proximity to the building will result in an abrupt change in the RPAS position.

To compare the results for each of the RPAS to one another, the results for U_{mean} limit versus the turbulence intensity, I_u , from Table 5.1 are shown in Figure 5.1 for the incremental wind speed gradient tests. The continuous wind speed gradient results have not been included as they do not represent a sustained wind speed. Trendlines, named U-I limit trendline for the remainder of this report, have been added to the plot to compare the broad effect of I_u on U_{mean} limit for the sRPAS size range.

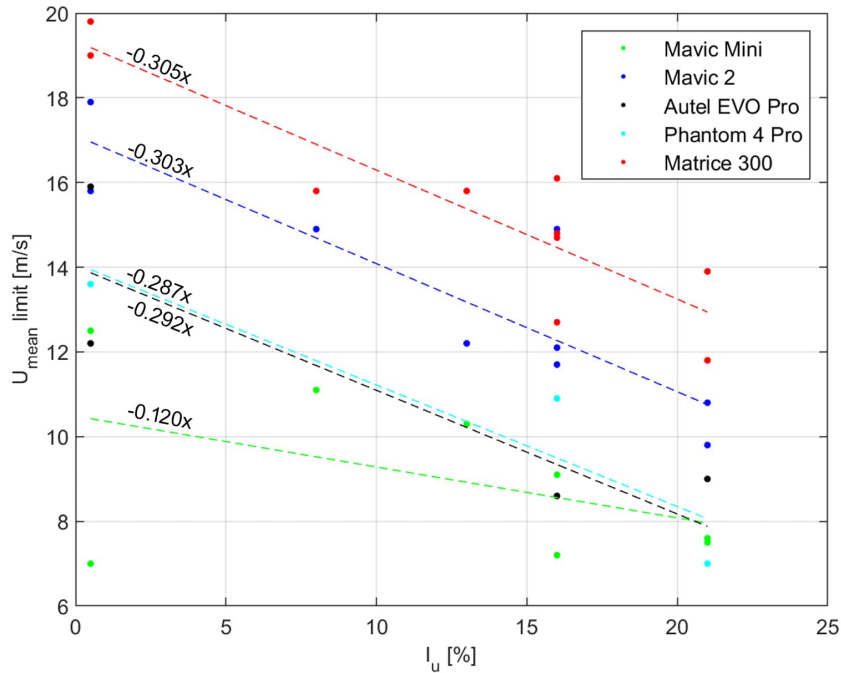


Figure 5.1: RPAS test results: wind speed limit versus turbulence intensity.

The U_{mean} versus I_u (U-I) limit trendlines show slopes of approximately $-0.3I_u$ for all RPAS except the Mavic Mini. The slope of the U-I limit trendline for the Mavic Mini is reduced, at $-0.1I_u$, as a result of the lower limit for the cross-wind configurations. For the Mavic Mini, at 0.249 kg, which is below the minimum weight for the sRPAS category, the mean wind speed played a larger factor in determining the limiting condition. This was most evident for the cross-wind orientation tests, where the Mavic Mini was significantly challenged. For cross-wind orientation the wind speed at which the RPAS could maintain position was reduced

to 7 m/s for smooth flow and turbulent flow conditions. For this RPAS a more consistent wind speed limit for the range of tested flow conditions was found in comparison to the other sRPAS, where the turbulence intensity level clearly influenced the wind speed limit.

Although not shown in this report, when the cross-wind results are omitted, the slope of the trend-line for the RPAS reduces by less than $0.04I_u$ for the other DJI models, and increases to $-0.25I_u$ for the Mavic Mini. The Autel model data set is not large enough to obtain a change in trend for omission of cross-wind orientation.

To understand why the RPAS sustained wind tolerance decreased with turbulence intensity, the time-series of the pitch- and roll - motor speed ratios was compared. During the wind tunnel test, at maximum operating efficiency, in smooth flow, the motor ratios were nearly constant and orientating the RPAS to hover against the wind. With the addition of turbulence, the ratio of the motor speeds had a larger variation due to the constantly changing moment on the RPA imposed by the constantly changing wind-loads. Figure 5.2 shows a time series comparison of the pitch- and roll-motor ratios of the Matrice 300 for a smooth flow condition (SMT-0-incr) and a configuration with 21% I_u (TU4-0-incr). Each time series plot is shown from the start of wind-on to the time at which the U_{mean} limit was determined.

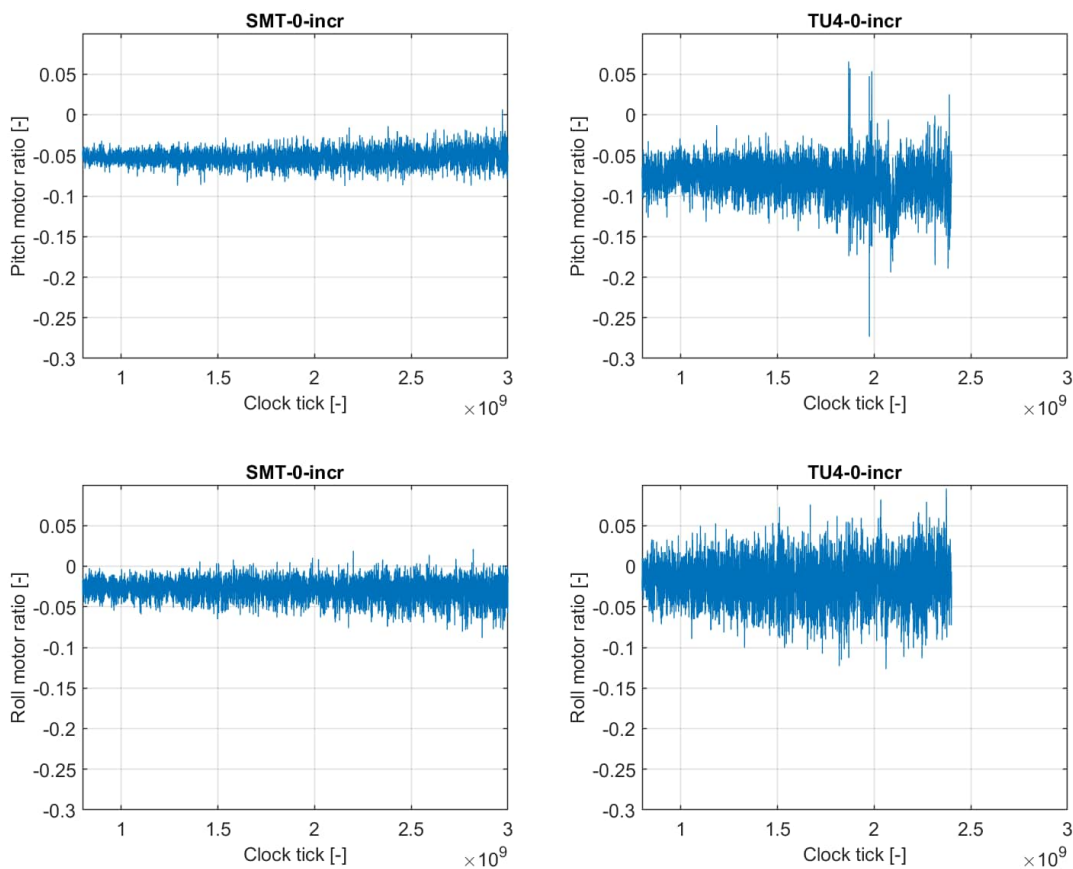


Figure 5.2: Pitch motor ratio and roll motor ratio for the Matrice 300 in SMT-0-incr and TU4-0-incr flow configurations. Left: smooth flow, right: turbulent flow.

From the Figure 5.2 plots it is evident that the variation in motor ratio of the RPA increases somewhat with an increase in wind speed, and significantly with an increase in turbulence. The pitch motor ratio for the smooth flow test oscillates between 0 and -0.1 at the U_{mean} limit, whereas for the TU4 test, with a turbulence intensity of 21% the pitch motor ratio oscillates between 0.05 and -0.25. The roll motor ratio for the smooth flow test also varies between 0 and -0.1 at the U_{mean} limit, whereas for the TU4 test, the roll motor ratio is oscillating between 0.1 and -0.13. For this case, the results suggest that the combination of the variation in pitch and roll caused a reduction in the wind speed tolerance from 19 m/s in smooth flow, to 12 m/s in turbulent flow which is significant because it is below the 15 m/s SWT specified by the manufacturer. The reduction in wind speed limit of the RPA caused by wind induced turbulence is expected to increase if an RPAS ascends through the urban canyon towards highly turbulent wakes of tall buildings. From the Part 1 urban flows test a turbulence intensity above 20% was found above low-rise buildings (<24 m) and up to heights within the wake of taller upstream buildings.

6. Evaluation of the Relationship Between the sRPAS Wind Speed Limit Results and the Urban Airflow Results

To gain an understanding of how the results from the speed and turbulence (U_{mean} and I_u) testing of the sRPAS relate to the levels of speed and turbulence measured within the flow-fields of the four Canadian city models, the U-I limit trendline results from Chapter 5 are compared to the urban results data sets from Chapter 3. A relationship between the sRPAS normalized U-I limit trendline and the normalized U_{mean} versus I_u data sets for the urban flow-fields are presented in this chapter.

For the urban flow-field results, by plotting the U_{mean} versus I_u values for each data point of each city flow-field, a full view of the relationship between speed and turbulence reveals the extent of the two variables for each of the city models tested. The plots in Figure 6.1 show a scatter of the urban airflow U_{mean} versus I_u data, where the marker colours denote the measurement height according to the colour bar legend.

All of the Figure 6.1 plots have a similar urban airflow results pattern with a convergence of the data points as turbulence increases. The top of the scatter plot shapes decrease in U_{mean} magnitude with an increase in I_u , similar to the U-I limit trendline for the sRPAS. The U-I limit trendline result for each sRPAS can be compared to the extents of the urban flow-field results to estimate at what wind speed each sRPAS will encounter instability due to atmospheric wind-speed and -turbulence for a given urban geometry.

The normalized U-I limit trendline for the Mavic 2 Zoom, sRPAS 'B', has been overlaid onto the Figure 6.1 plots. Both data sets, including the data points used to determine the U-I limit trendline and the urban airflow wind speed, U_{mean} , were normalized by the reference height wind tunnel speed, for each city. For the sRPAS data the absolute value of the sRPAS wind speed limit results were divided by the average reference height wind tunnel speed, whereas for the urban flows data, each data point result was normalized using the mean reference wind speed from the corresponding test.

Since the data points for the sRPAS test results had a deviation of up to ± 0.1 , 'B trend+0.1' and 'B trend-0.1' have been added to the Figure 6.1 plots to account for variation caused by RPA orientation and/or other possible testing uncertainties. The trendlines have been placed above the urban flows data so that the 'B trend-0.1' intersects with the highest scatter marker. If the 'B trend' lines are positioned at a height where 'B trend-0.1' is at or above all of the data points in the scatter plot it can be used to estimate a wind speed at which the sRPAS will avoid flight control or instability issues due to mean wind speed or turbulence. A method for using the height of the trendline to calculate the minimum atmospheric wind speed limit for safe flying is explained in the following.

At the y-intercept of the 'B trend' curve, denoted in Figure 6.1 by the 'X' on the y-axis, the normalized value can be used to determine the relative dimensional wind speed at other heights,

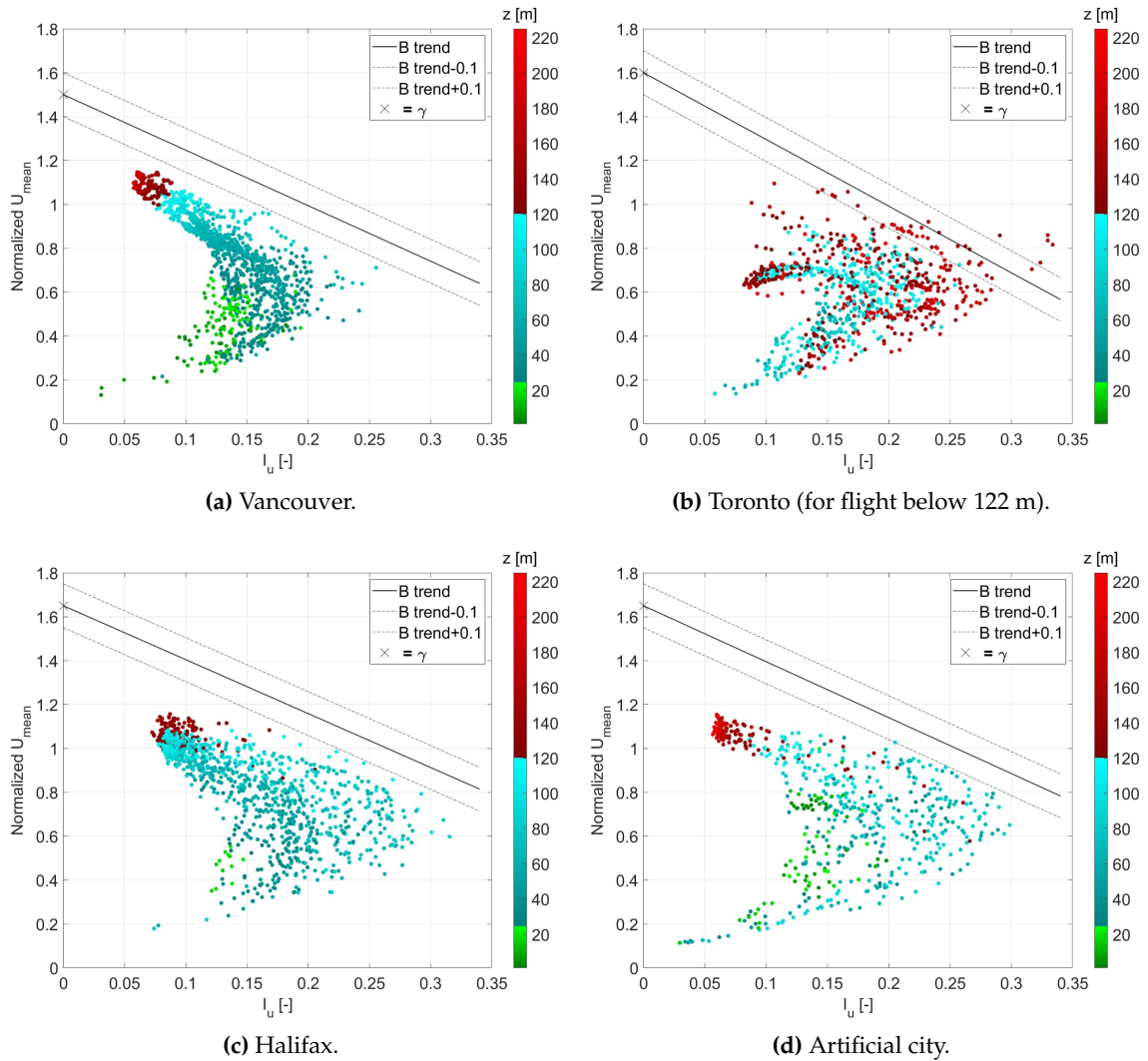


Figure 6.1: Urban wind-speed and -turbulence instability avoidance graph for the Mavic 2 Zoom.

including weather station height, using a two-step process:

1. Convert the smooth flow sRPAS wind speed limit to a wind speed at the normalized U_{mean} of 1.0 by using the y-intersect value as a ratio. This will determine the wind speed at the full scale equivalent to the sRPAS altitude limit of 122 m because it is the height at which the urban airflow wind speed was normalized.
2. Using the theoretical atmospheric boundary layer curve, or power law curve, convert the wind speed at 122 m to the estimated wind speed at 10 m above ground for open terrain where weather stations (airports) are typically located. The wind speed at the weather station represents the maximum reported wind speed in which the RPAS should be operated to avoid instabilities due to speed and turbulence combinations at higher altitudes within the urban environment.

Step 1 equation:

$$U_{N_{1.0}} = U_{122} = \frac{SMT_{Limit}}{\gamma} \quad (6.1)$$

where $U_{N_{1.0}}$ and U_{122} are the calculated relative dimensional sRPAS wind speed limit at 122 m above ground, SMT_{Limit} is the smooth flow condition value of the trendline (not the single point U_{mean} limit test result), 'B trend', at the y-intercept ($I_u = 0$) found from the wind tunnel test results and γ is the normalized value of U_{mean} at the y-intercept which is found by placing the 'B trend-0.1' trendline, which accounts for deviation in the test results, at a height that avoids crossing through the urban airflow data.

Step 2 equation:

The Chapter 3 urban airflow wind speed results showed that the wind speed at a height of 122 m does persist into the airflow above urban centres representing Canadian cities if undisturbed by building wakes and can therefore be used as a cross-terrain wind speed reference between urban wind speeds and wind speeds outside of the city in open terrain. Therefore, a relationship between the dimensional U_{122} and the wind speed at a weather station height, which is typically 10 m above ground, can be calculated using the widely accepted power-law curve for estimating atmospheric boundary layer wind speed as follows (Davenport, 1960):

$$U_z = U_{122} \left(\frac{z}{122} \right)^\alpha \quad (6.2)$$

$$U_{10} = U_{122} \left(\frac{10}{122} \right)^{0.16} = \frac{U_{122}}{1.5} \quad (6.3)$$

where U_z is the wind speed at an above ground height, z , U_{122} is the dimensional wind speed from Equation (6.1) and α is the power law exponent which is 0.16 for open terrain where airport weather stations are located. For weather stations, where the wind speed is typically measured at 10 m above ground, Equation (6.2) can be simplified as shown in Equation (6.3), to estimate a wind speed at weather station height, U_{10} .

A schematic of the power law curves of the atmospheric boundary layer wind speed profile with respect to the relative terrains are shown in Figure 6.2, where U_{122} is a common value for Step 1 and Step 2.

For the Mavic 2 Zoom, the calculations and results from the Figure 6.1a U-I limit trendline, 'B trend', for Vancouver, in m/s, are:

$$U_{N_{1.0}} = U_{122} = \frac{17.1}{1.5} = 11.4 \quad (6.4)$$

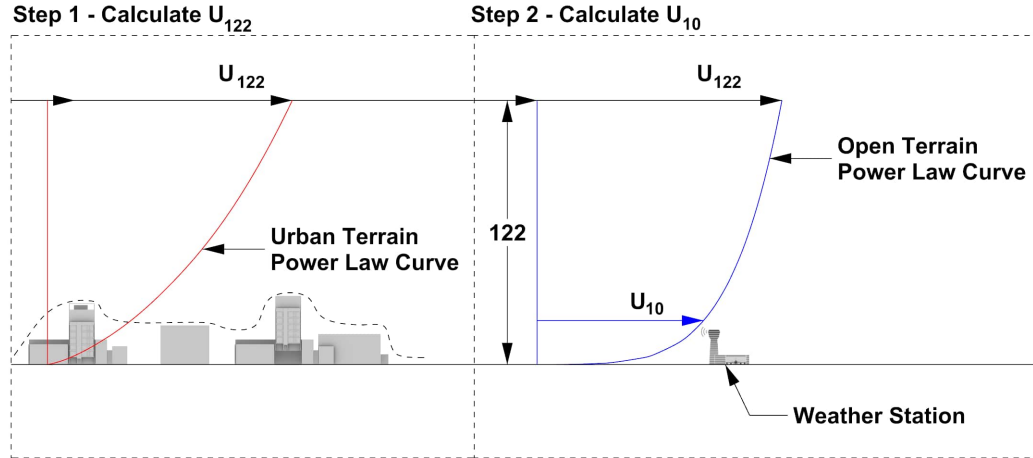


Figure 6.2: Schematic of urban and open terrain wind speed profile relationship used for Equation (6.2) and Equation (6.3) .

$$U_{10} = U_{122} \left(\frac{10}{122} \right)^{0.16} = \frac{U_{122}}{1.5} = \frac{11.4}{1.5} = 7.6 \quad (6.5)$$

The results for the Mavic 2 Zoom suggest that to avoid wind-speed and -turbulence limiting conditions for flight within the urban flow-field at the Vancouver model site at an altitude limit of 122 m, the operator should not fly when wind speeds are predicted to be above 7.6 m/s (27.4 km/h) from a local weather station hourly report. This result is below the manufacturer's specified sustained wind speed limit of 10.6 m/s and the wind tunnel tests with low turbulence. This is because the results of the method are controlled by the urban data points with higher turbulence levels and the additional safety factor added by the 'B trend -0.1' line which sets the height of the U-I trendline. However, considering the scatter of the sRPAS results, this conservative method can be justified and highlights that the wind tolerances specified by manufacturers need to include turbulence intensity levels or provide a U-I trendline so that operators can plan for specific flight environments where turbulent wind is a factor.

Table 6.1 lists the urban wind-speed and -turbulence instability avoidance results for all sRPAS reported in Chapter 5, where γ was determined for each RPAS for each city. Since Toronto had a significant number of scatter plot data points above 122 m, whereas the other cities did not, two trendline results for Toronto were calculated. Toronto results are shown for placement of the U-I limit trendline including only the data for measurement heights below 122 m and for all of the data points including heights up to 220 m.

When comparing the results of γ for the four cities, it can be seen that for the Toronto results, including only data points below 122 m, the trendline intersects the data scatter at a lower γ than for the Halifax and Artificial city results. Figure 6.1 shows that the cyan markers in the Toronto plot, representing data points below an altitude of 122 m, are lower than for the other cities. It appears that the higher building density of the taller buildings within that height cause a reduction in wind speed in comparison to the other city results, lowering the

minimum height of the U-I limit trendline.

In general, the combination of the shape of the urban airflow data scatter and the slope of the sRPAS U-I limit trendline determines the safe U_{10} atmospheric wind speed. For all sRPAS models except the Mavic Mini, the intersect of the trendline with the scatter data occurs at a range of between 0.15 and 0.30 I_u . This range includes the I_u at which most of the sRPAS were found to reach their manufacturer's specified sustained wind speed tolerance shown in Chapter 5 Table 5.1.

Table 6.1: Urban wind-speed and -turbulence instability avoidance results.

RPAS Tag	RPAS Model	City	γ	Trendline SMT_{Limit} [m/s]	Calculated $U_{N_{1,0}}(U_{122})$ [m/s]	U_{10} [m/s]	U_{10} [km/h]
A	DJI Mavic Mini	VAN	1.35	10.5	7.8	5.2	18.6
		TOR below 122 m	1.20	"	8.7	5.8	21.0
		TOR all data	1.40	"	7.5	5.0	18.0
		HAL	1.35	"	7.8	5.2	18.6
		ART	1.35	"	7.8	5.2	18.6
B	DJI Mavic 2 Zoom	VAN	1.50	17.1	11.4	7.6	27.4
		TOR below 122 m	1.60	"	10.7	7.1	25.7
		TOR all data	2.00	"	8.6	5.7	20.5
		HAL	1.65	"	10.4	6.9	24.9
		ART	1.65	"	10.4	6.9	24.9
C	Autel EVO II Dual Pro	VAN	1.50	14.0	9.3	6.2	22.4
		TOR below 122 m	1.55	"	9.0	6.0	21.7
		TOR all data	1.95	"	7.2	4.8	17.2
		HAL	1.60	"	8.8	5.8	21.0
		ART	1.65	"	8.5	5.7	20.4
D	DJI Phantom 4 Pro	VAN	1.50	14.1	9.4	6.3	22.5
		TOR below 122 m	1.55	"	9.1	6.1	21.8
		TOR all data	1.90	"	7.4	4.9	17.8
		HAL	1.60	"	8.8	5.9	21.1
		ART	1.65	"	8.5	5.7	20.5
E	DJI Matrice 300	VAN	1.50	19.3	12.9	8.6	30.9
		TOR below 122 m	1.60	"	12.1	8.1	29.0
		TOR all data	1.95	"	9.9	6.6	23.8
		HAL	1.65	"	11.7	7.8	28.1
		ART	1.65	"	11.7	7.8	28.1

The Table 6.1 U_{10} wind speed results for all sRPAS models and all cities are lower than the manufacturers specified sustained wind speed tolerance. The wind speeds at the 10 m above ground height, U_{10} , are between 5.2 m/s (18.6 km/h) for the Mavic Mini and 8.6 m/s (30.9 km/h) for the Matric 300 which fit within the moderate breeze to fresh breeze categories according to the mean wind speeds on the Beaufort Scale (Royal Meteorological Society, 2022), which are relatively light winds, but will be approximately 1.5 times higher at the sRPAS altitude limit of 122 m and therefore are not considered overly conservative with respect to the sRPAS wind tunnel test results for the respective models.

The reason that the Table 6.1 U_{10} wind speed results are lower than the U_{mean} limit results from the wind tunnel testing reported in Chapter 5 Table 5.1 is that the data points within the urban flow-field scatter have a higher I_u than for the flow conditions that the sRPAS group were tested. The difference between the U_{mean} limit and the U_{10} wind speed is a result of the U-I trendline slope for each sRPAS, where the Mavic Mini has the smallest variation and the Matrice 300, with the steepest slope, shows the largest variation.

For the Mavic Mini, the intersection of the reduced slope of the U-I limit trendline with the scatter of data occurred at low I_u and higher U_{mean} urban airflow results. For the light-weight Mavic Mini, wind speed is of greater influence on performance than I_u , due to the impact of form drag in comparison to thrust as noted in Chapter 5. This contrast of the U-I trendline/scatter intersect location to that of the heavier more powerful sRPAS shows the effectiveness of the U-I limit trendline intersection method, which factors into the process, the flow condition that had the most impact on the measured RPAS wind speed limit.

The variation in results between city models for each sRPAS ranges from 0.56 to 0.78 m/s (2.0 to 2.8 km/h) for heights below 122 m. This range is not large in comparison to hourly changes in atmospheric wind speed or wind gust predictions, suggesting a broad approach to limits for Canadian cities with respect to the combination of wind-speed and -turbulence for that height limit, is not unreasonable.

The results in Table 6.1 for Toronto for altitudes including data point heights above 122 m show that a larger γ is required for the U-I trendline to intersect with the high wind speed, U_{mean} , and high turbulence intensity, I_u , caused by the taller high-rise building wakes. Figure 6.3 shows how the 'B trend' line for the Mavic 2 Zoom has a γ of 2.0 to avoid the turbulence of over $0.3I_u$, for which U_{mean} is also high at approximately 0.8. The results for the high density and high-rise model representing Toronto have shown significant differences between flying within the higher density region of the street canyons which is mostly below 122 m and the more sparsely spaced tall high-rise region above 122 m where the wind speed is higher and the roughness of the tops of the buildings cause an increase in turbulence intensity. The difference in results with respect to measurement height suggests that altitude is a significant factor for determining flight stability limits within the urban environment above Canadian cities with tall high-rise buildings.

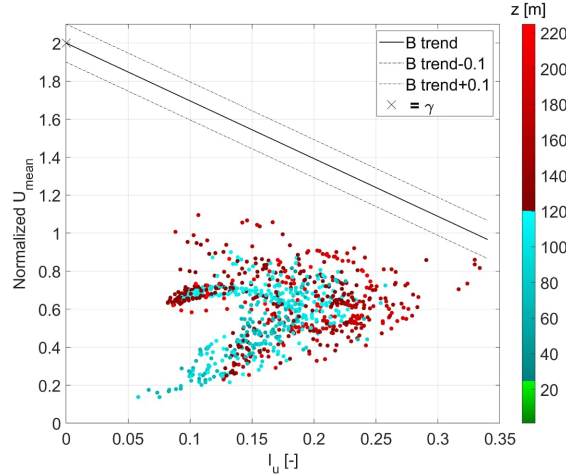


Figure 6.3: Urban wind-speed and -turbulence instability avoidance graph for the Mavic 2 Zoom: Toronto, all data points.

For the sRPAS category, where the nominal altitude limit is 122 m, a recommendation can be made for guidance on safe urban operations for the avoidance of instability caused by turbulence if sRPAS manufacturers were required to use a standardized method for evaluating the sustained wind speed tolerance. From the results of this study, the consistent trend of the wind speed limits of the tested sRPAS quadcopters (not the Mavic Mini), and the small variation between results when evaluated against the urban airflow results presented in Table 6.1, a sustained wind speed limit for smooth airflow conditions ($I_u = 0$) could be used to determine a maximum operating wind speed reported by a local weather station for a nearby urban environment as follows:

$$U_{10} = \frac{SMT_{Limit}}{\gamma \times 1.5} \quad (6.6)$$

which combines Equation (6.1) and Equation (6.3). To simplify the equation further, a maximum γ of 1.65, found for Vancouver and Halifax shown in the Table 6.1 results could be integrated into the equation as follows:

$$U_{10} = \frac{SMT_{Limit}}{2.5} \quad (6.7)$$

If a manufacturer finds the method overly conservative, a U-I trendline could be provided by the manufacturer to verify a specific γ for an sRPAS model for the U_{10} calculation. This revised U-I trendline would need to be based on results derived from a well-controlled and standardized experiment. The new γ would be found by placing a trendline, including offset tolerance for test result scatter similar to 'B trend-0.1', above a curve representing the upper limit of the U_{mean} to I_u relationship found for the Canadian city urban airflow tests. A graphical sample is shown in Figure 6.4.

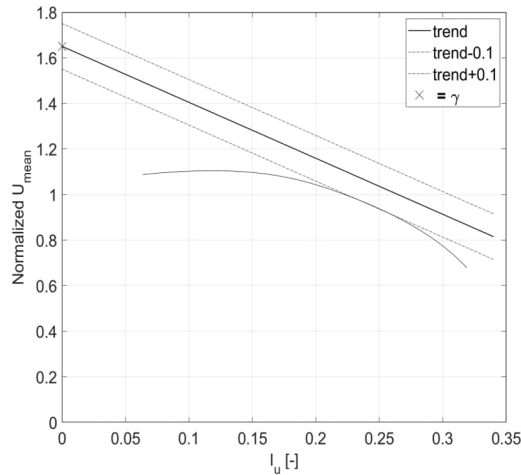


Figure 6.4: Sample urban wind-speed and -turbulence instability avoidance graph.

To build confidence in the sRPAS trendline/urban scatter-data intersect approach for instability caused by wind -speed and -turbulence any future testing during the next phase of this project should include evaluation of the method for any additional sRPAS models.

The results in this Chapter are presented with respect to weather station reports for the sRPAS tested using the U-I limit trendline, but do not evaluate a safe wind speed limit for other urban airflow types such as an abrupt change in direction, building wake shear or rooftop vortices. The next phase of work planned for this project will include the remaining urban airflow features expected to impact RPAS urban flight stability, adding to the results in this report to provide a more complete conclusion on the effects of urban airflow on sRPAS.

7. Summary and Next Steps

7.1 Urban Airflow Characterization

Analysis of the 3 m × 6 m Wind Tunnel test urban airflow measurements from four model cities for the speed (S_1) and turbulence (T) components of the S_1 D S_2 T V urban flow characteristics has resulted in the following conclusions:

- In comparison to the simulated ABL wind speed profile measured upstream of the city models, the wind speed is slowed within the urban environment except in some locations where no upstream building is present. Additionally, for many cases where no upstream building was directly in the path of the measured location, the flow was also slowed by the overall re-direction of flow caused by wake interaction within the city canyons.
- For each of the four city models, the wind speed measured upstream of the urban centre at the reference height of 122 m full scale (400 ft) persisted into the core of the city model for measurement locations with no upstream building. Therefore, estimating wind speeds at 122 m above ground within the urban environment using local airport reports is a reasonable method.
- The normalized wind speed within the urban flow-fields of the tested models is highly variable with a maximum U_{mean} range of between 0.16 and 1.0 for a height range of between 3 m and 122 m above ground.
- For an RPAS flight path that passes through a building wake within the near-wake region, the mean wind speed can increase by up to 3 times over a distance of 18 m, when transitioning from the slowed flow within the recirculation region to the outer shear layers of the wake.
- For all city models, the turbulence intensity, I_u , of the wind speed had a maximum of between 26% and 33%, where the extreme cases were found within the RSL and were located within the side-wall or rooftop wake region of tall buildings.
- The maximum I_u measured within the flow-field of the four city models was found in the wake of small features at the top of a tall building or within the large overall single- or multi-wake of tall buildings, where the lateral location was dependent on wind angle and the cross-section size of the high intensity level was dependent on urban feature size.

Analysis of the urban flows data for the remaining flow types, D S_2 and V is planned for the next phase of this project. The model scale D S_2 and V results will be converted to full scale magnitudes and characteristics will be used to develop simulated urban airflow conditions for the next phase of sRPAS wind tunnel testing.

7.2 sRPAS Wind Tunnel Test

Testing of five small RPAS in the 3 m × 6 m Wind Tunnel for the urban airflow types speed and turbulence, S_1 and T, successfully demonstrated the reactions of the models to high wind speeds and highlighted the effects of urban airflow turbulence intensity on sRPAS. The key findings from the wind tunnel test program include:

- At the measured wind speed limit, a combination of wind speed and turbulence caused the sRPAS to gradually slip downstream with erratic shifting in attitude but without change in overall heading.
- When compared to the manufacturers specifications for sustained wind speed tolerance, the wind tunnel test results showed inconsistency between manufacturers, where some results were lower and some results were higher than the specification. This discrepancy indicates that a standard method for evaluating sRPAS for wind conditions is not consistent within the industry.
- In general, the sRPAS (excluding the under-weight Mavic Mini) sustained wind speed limit, or $U_{mean\ limit}$, decreased at a rate of $0.3 \times I_u$ when flying within the turbulence range of 8% to 21% for the group of sRPAS tested.
- The effect of turbulence, I_u , on the RPAS was a reduction in sustained wind speed tolerance, or $U_{mean\ limit}$, likely due to loss of attitude controllability caused by the continually changing control moment of the RPA which was required by the aircraft to maintain stability and position.

The 3 m × 6 m Wind Tunnel testing fulfilled the test program goals for the evaluation of speed and turbulence for a range of sRPAS. The challenges of testing within the confines of the 3 m × 6 m Wind Tunnel were surmountable for this test, but for RPAS at the heavier end of the sRPAS category, a larger facility would reduce the risk of collision for flow conditions with a higher risk of RPAS flight instability than speed and turbulence. For the next phase of sRPAS testing consideration should be made for a larger test facility for the urban airflow types, shear, direction and vorticity.

7.3 Evaluation of sRPAS Wind Tunnel Results when Compared to the Urban Airflow Results

A method has been presented that compares the sRPAS wind tunnel test results wind-speed and -turbulence trendlines to the mean wind-speed and -turbulence results from the urban airflow wind tunnel test of the four representative Canadian cities. The method translates the sRPAS results into a maximum weather station report wind speed, U_{10} , measured outside of a city, that is predicted to prevent RPAS instability caused by urban wind-speed and -turbulence by superimposing the sRPAS results trendline at the extremes of the urban airflow results. The resulting prediction of the U_{10} limits for the five sRPAS models and four city models showed that:

- When compared to the extreme values of wind-speed and -turbulence, for the sRPAS to

fly safely within the urban flow-fields at the altitude limit of 122 m, the translated wind speed at the height of a weather station, U_{10} , is lower than the manufacturers specified sustained wind speed tolerance.

- The variation in the U_{10} values between city models for each sRPAS model was less than 0.78 m/s (2.8 km/h) for heights below 122 m, which is small in comparison to mean hourly changes in wind speed or gust predictions, suggesting a broad approach to limits for Canadian cities with respect to the combination of wind-speed and -turbulence for that height limit, is not unreasonable.
- The results for the high density and high-rise model representing Toronto have shown significant differences between flying within the higher density region of the street canyons which is mostly below 122 m and the more sparsely spaced tall high-rise region above 122 m where the wind speed is higher and the roughness of the tops of the buildings cause an increase in turbulence intensity. The difference in results with respect to measurement height suggests that altitude is a significant factor for determining flight stability limits within the urban environment above Canadian cities with tall high-rise buildings.
- A simplified method has been explained and is recommended for support of safe sRPAS urban operations that requires manufacturers to provide a wind speed limit at weather station measurement height, U_{10} , that accounts for avoidance of Canadian urban airflow wind-speed and -turbulence that has been shown to cause sRPAS instability.

The wind tunnel test results, including the urban airflow results and the sRPAS flight test results, along with the comparison of those results to one another have shown the importance of including both wind-speed and wind-turbulence in the prediction of stability limits for urban flight conditions. For the next phase of testing of the remaining flow types, the correlation of speed to each flow type should be included.

References

- Al Labbad, M. (2021), "The Effects of Urban Settings on Airflow Characteristics for Urban Air Mobility Applications," Master's thesis, Carleton University.
- Bai, H. (2018), "Dependence of square cylinder wake on Reynolds number," *Physics of Fluids*, **30**, pp. 015102.
- Barber, H. and Wall, A. (2020), "Urban Airflow: What Drone Pilots Need to Know," No. LTR-AL-2020-0075, *National Research Council Canada*.
- Burggräf, P., Martinez, A. R. P., Roth, H. and Wagner, J. (n.d.), "Quadrotors in factory applications: design and implementation of the quadrotor's P-PID cascade control system."
- CAAM and NEXA Advisors (2021), "Advanced Air Mobility Comes to Toronto," *AAM White Paper Series*, October, 2021.
- Davenport, A. (1960), "Wind Loads on Structures," No. 88, *National Research Council of Canada Division of Building Research*.
- Davenport, A. G. (1961), "The spectrum of horizontal gustiness near the ground in high winds," *Quarterly Journal of the Royal Meteorological Society*, **87**, pp. 194–211.
- Davenport, A. G. (2007), *WIND TUNNEL TESTING: A GENERAL OUTLINE*, The University of Western Ontario, Faculty of Engineering Science.
- Deschamps, T. (2021), *Toronto hospitals, Quebec company behind world's first delivery of lungs by drone*, <https://www.ctvnews.ca/sci-tech/toronto-hospitals-quebec-company-behind-world-s-first-delivery-of-lungs-by-drone-1.5619862>.
- Hertwig, D., Gough, H. L., Grimmond, S., Barlow, J. F., Kent, C. W., Lin, W. E., Robins, A. G. and Hayden, P. (2019), "Wake characteristics of tall buildings in a realistic urban canopy," *Boundary-Layer Meteorology*, **172**, pp. 239–270.
- Hooper, J. D. and Musgrove, A. R. (1997), "Reynolds Stress, Mean Velocity, and Dynamic Pressure Measurement by a Four-Hole Pressure Probe," *Experimental Thermal and Fluid Science*, **15**, pp. 375–383.
- Irwin, H. P. A. H. (1979), "Design and Use of Spires for Natural Wind Simulation," *National Research Council of Canada - Laboratory Technical Report No. LTR-LA-233*.
- Irwin, P., Garber, J. and Ho, E. (2005), "Integration of Wind Tunnel Data with Full Scale Wind Climate," *Tenth Americas Conference on Wind Engineering*.

- Kulisch, E. (2021), *Air Canada Cargo embraces drone delivery as growth area*, <https://www.freightwaves.com/news/air-canada-cargo-embraces-drone-delivery-as-growth-area>.
- Kuznetsov, S., Butova, A. and Pospisil, S. (2016), "Influence of placement and height of high-rise buildings on wind pressure distribution and natural ventilation of low- and medium-rise buildings," *International Journal of Ventilation*, **15**, pp. 253–266.
- Nedić, J., Ganapathisubramani, B. and Vassilicos, J. (2013), "Drag and near wake characteristics of flat plates normal to the flow with fractal edge geometries," *Fluid Dynamics Research*, **45**, pp. 061406.
- Royal Meteorological Society (2022), *The Beaufort Scale*, <https://www.rmets.org/resource/beaufort-scale>.
- Transport Canada (2021), *Urban Airflow: What Drone Pilots Need to Know*, <https://tc.canada.ca/en/aviation/drone-safety/tips-best-practices-drone-pilots/urban-airflow-what-drone-pilots-need-know>.
- Turbulent Flow Instrumentation (2022), *Getting Started Series 100 Cobra Probe*, [https://www.turbulentflow.com.au/Downloads/Getting Started - Cobra Probe.pdf](https://www.turbulentflow.com.au/Downloads/Getting%20Started%20-%20Cobra%20Probe.pdf).
- Wall, A., Lee, R. and Barber, H. (2020), "Analysis of Fast-Response Cobra Probe Data in Highly Turbulent Wake Flows," <https://nrc-publications.canada.ca/eng/view/object/?id=9147610b-dbe9-443b-b77a-cbb15eb3a28e>.

A. Appendix A

Table A.1: Test matrix: Vancouver.

Configuration Name	ABL Profile	Cobra Angle [deg]	Height Range [FS m]
VAN:40:CTR:0:0	SUB	0	32 - 182
VAN:60:CTR:0:0	SUB	0	32 - 182
VAN:140:CTR:0:0	SUB	0	32 - 182
VAN:160:CTR:0:0	SUB	0	32 - 182
VAN:180:CTR:0:0	SUB	0	32 - 182
VAN:200:CTR:0:0	SUB	0	32 - 182
VAN:270:CTR:0:0	SUB	0	32 - 182
VAN:270:AVE:620:-60	SUB	0	3 - 153
VAN:270:AVE:620:180	SUB	0	3 - 153
VAN:270:AVE:620:420	SUB	0	3 - 153
VAN:270:AVE:630:660	SUB	0	3 - 153
VAN:270:AVE:630:860	SUB	0	3 - 153
VAN:300:VOR:-38:-586	OPS	0	3 - 105
VAN:300:VOR:22:-586	OPS	0	3 - 105
VAN:300:VOR:82:-586	OPS	0	3 - 105
VAN:300:VOR:82:-576	OPS	0	3 - 105
VAN:300:VOR:82:-566	OPS	0	3 - 105
VAN:300:VOR:82:-556	OPS	0	3 - 105
VAN:300:VOR:82:-546	OPS	0	3 - 105
VAN:300:VOR:82:-536	OPS	0	3 - 105
VAN:300:VOR:82:-526	OPS	0	3 - 105
VAN:90:SHE:-630:-390	SUB	0	9 - 63
VAN:90:SHE:-630:-410	SUB	0	9 - 63
VAN:90:SHE:-630:-430	SUB	0	9 - 63
VAN:90:SHE:-630:-450	SUB	0	9 - 63
VAN:270:VPA:60:860	SUB	0	3 - 33 ^t
VAN:270:HPA:60:0,180,420,660	SUB	0	110 ^t
VAN:270:HPA:60:0,180,420,660	SUB	0	135
VAN:270:HPA:60:0,180,420,660	SUB	0	160
VAN:270:HPA:60:0,180,420,660	SUB	0	185

^t Data collected for stationary and moving probes.

Table A.2: Test matrix: Halifax.

Configuration Name	ABL Profile	Cobra Angle [deg]	Height Range [FS m]
HAL:0:CTR:-334:-199	OPS	0	33 - 108
HAL:20:CTR:-235:-299	OPS	0	33 - 108
HAL:340:CTR:-380:-131	OPS	0	33 - 108
HAL:300:CTR:-365:205	OPS	0	33 - 108
HAL:280:CTR:-283:319	OPS	0	33 - 108
HAL:159:AVE:393:-960	OPS	0	30 - 150
HAL:159:AVE:393:-720	OPS	0	30 - 150
HAL:159:AVE:393:-480	OPS	0	30 - 150
HAL:159:AVE:393:-240	OPS	0	60 - 150
HAL:159:AVE:393:0	OPS	0	60 - 150
HAL:159:AVE:393:240	OPS	0	60 - 150
HAL:159:AVE:393:480	OPS	0	60 - 150
HAL:159:AVE:393:720	OPS	0	60 - 150
HAL:159:AVE:393:960	OPS	0	90 - 150
HAL:200:VOR:-530:150	OPS	0	84 - 120
HAL:200:VOR:-530:160	OPS	0	84 - 120
HAL:200:VOR:-530:170	OPS	0	84 - 120
HAL:200:VOR:-530:180	OPS	0	84 - 120
HAL:200:VOR:-530:190	OPS	0	84 - 120
HAL:200:VOR:-530:200	OPS	0	84 - 120
HAL:200:VOR:-530:210	OPS	0	84 - 120
HAL:115:SHE:-753:651	OPS	0	72 - 132
HAL:115:SHE:-900:180	OPS	0	72 - 132
HAL:115:SHE:-938:36	OPS	0	72 - 132
HAL:115:SHE:-863:-282	OPS	0	72 - 132
HAL:270:VPA:720:780	OPS	0	15 - 45 ^t
HAL:270:HPA:720:-660,-420,-180,60,300,540,780	OPS	0	150 ^t
HAL:270:HPA:720:-660,-420,-180,60,300,540,780	OPS	0	175
HAL:270:HPA:720:-660,-420,-180,60,300,540,780	OPS	0	200
HAL:270:HPA:720:-660,-420,-180,60,300,540,780	OPS	0	225
HAL:270:HIL:-1340:780	OPS	0	84 - 114
HAL:270:HIL:-1340:540	OPS	0	84 - 114
HAL:270:HIL:-1340:300	OPS	0	84 - 114
HAL:270:HIL:-1340:60	OPS	0	84 - 114
HAL:270:HIL:-1340:-180	OPS	0	84 - 114
HAL:270:HIL:-1340:-420	OPS	0	84 - 114
HAL:270:HIL:-1340:-660	OPS	0	84 - 114

^t Data collected for stationary and moving probes.

Table A.3: Test matrix: Artificial city.

Configuration Name	ABL Profile	Cobra Angle [deg]	Height Range [FS m]
ART:0:CTR:0:0	SUB	0	8 - 203
ART:90:CTR:0:0	SUB	0	8 - 203
ART:135:CTR:0:0	SUB	0	8 - 203
ART:270:CTR:0:0	SUB	0	8 - 203
ART:315:CTR:0:0	SUB	0	8 - 203
ART:90:JET:-30:-400	SUB	0	53 - 90
ART:90:JET:-30:-390	SUB	0	53 - 90
ART:90:JET:-30:-380	SUB	0	53 - 90
ART:90:JET:-30:-370	SUB	0	53 - 90
ART:90:JET:-30:-360	SUB	0	53 - 90
ART:90:JET:-30:-350	SUB	0	53 - 90
ART:90:MD1:186:770	SUB	0	3 - 96
ART:90:MD2:186:684	SUB	0	3 - 96
ART:90:MD3:186:684	SUB	0	3 - 96
ART:90:MD4:186:684	SUB	0	3 - 96
ART:160:VPA:750:540	SUB	0	3 - 71 ^t
ART:160:HPA:750:300,60,-180,-420,-660*	SUB	0	71 ^t
ART:160:HPA:750:300,60,-180,-420,-540,-660	SUB	0	89
ART:160:HPA:750:300,60,-180,-420,-540,-660	SUB	0	107
ART:315:CHA:480:584	SUB	-25, 0 ,25	15 - 90
ART:315:CHA:480:564	SUB	-25, 0 ,25	15 - 90
ART:315:CHA:480:544	SUB	-25, 0 ,25	15 - 90

^t Data collected for stationary and moving probes. * Data collected for y = -540 used from VPA configuration.